Design of an Electronically-Actuated Gas Lift Safety Valve
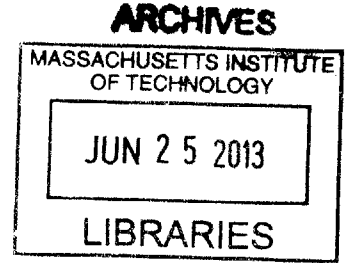
By

Changkuan Yu

B.S., Stanford University (2011)

Submitted to the Department of Mechanical Engineering

in partial fulfillment of the requirements for the degree of

Masters of Science in Mechanical Engineering

at the

MASSACHUSETTS INSTITUTE OF TECHNOLOGY

June 2013

Author. . . . . , ...

Department of Mechanical Engineering

May 14, 2013

Certified by. . . . ./. . . . . -, , ...

Franz Hover

Finmeccanica Career Development Associate Professor

Thesis Supervisor

Accepted by. . . . .

David E. Hardt

Graduate Officer, Department of Mechanical Engineering

Design of an Electronically Actuated Gas Lift Safety Valve

By

Changkuan Yu

Submitted to the Department of Mechanical Engineering

on May 14, 2013, in partial fulfillment of the

requirements for the degree of

Masters of Science in Mechanical Engineering

Abstract

Gas lift valves are widely used in oil production fields to pump recycled gas and nitrogen into the production tubing, to sustain production by aerating the oil and lifting it to the ground or sea surface. Today's industry standard, a pressure-actuated valve, is susceptible to various modes of failure, including corrosion and jamming. Safety mechanisms are needed to seal the valve in case of a backflow event, in which oil flows backward through the production tubing. Since human monitoring is difficult to implement at deep level underground, these safety mechanisms have to be highly sensitive and autonomous.

This thesis documents the design of an electronically-actuated gas lift safety system that builds on a prior invention based on shape-memory alloy, but, among other features, can handle the slowly changing temperature conditions downhole. The newly-designed control circuit is integrated into the original shape memory alloy (SMA) scheme. The selection criteria and features of various sensors in this circuit are reviewed in relation to oil's physical and chemical characteristics. System functionality is proved through model-scale prototype testing within a controlled environment. At the same time, the system is modeled with heat transfer and structural analysis to predict its behavior in different environments with air or water , or their mixture with oil. Overall, our concept satisfies many of the key operational needs in artificial gas lift.

Thesis Supervisor: Franz Hover

Title: Finmeccanica Career Development Associate Professor

Acknowledgments

Contents

List of Figures

List of Tables

Chapter 1

Introduction

1.1   Petroleum Production and Consumption

Fossil fuels are a major energy source on earth: about 90% of the world's total energy is provided by coal, gas, and petroleum. Petroleum is used widely in power plants, transportation, and heat generation; in addition, the chemical products derived from petroleum, such as plastics and carbon fibers, are also used in other industries and applications. Among these fossil fuels, oil is especially critical to the US economy. It accounts for 40% of the total US energy consumption, including 94% of transportation consumption and 40% of industry consumption [12]. As a result, oil supply security has become a cornerstone of US national security in both the economy and military defense and has led to several military conflicts in oil production regions such as the Persian Gulf in the first decade of the 21st century.
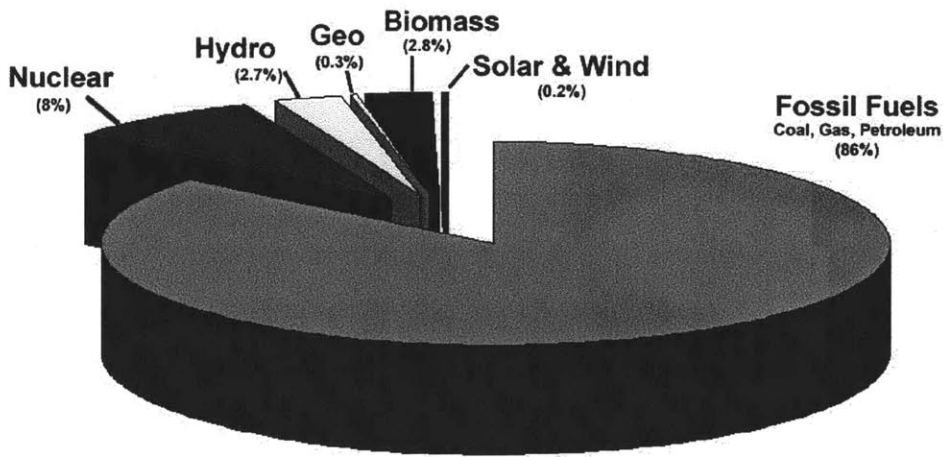
Source: International Energy Agency (2004)

Figure 1-1:   Energy source distribution around the world

The use of fossil fuels has arguably caused considerable global climate change over the 200 years since the first Industrial Revolution and these fuels are increasingly being replaced by new

sustainable clean energy, e.g. wind, solar, nuclear, and hydro power. Nevertheless, the dominant position of fossil fuels in the US economy will remain for at least the next 50 years. Therefore, more resources and technology than ever before are being applied to search for more oil reservoirs and to increase, or at least sustain, the production rate of the current ones.

Rank	Country	Production
1	Saudi Arabia	10,665
2	Russia	9,677
3	United States	8,330
4	Iran	4,148
5	China	3,845
6	Mexico	3,707
7	Canada	3,288
8	United Arab Emirates	2,945
9	Venezuela	2,803
10	Norway	2,786
11	Kuwait	2,675
12	Nigeria	2,443
13	Brazil	2,167
14	Algeria	2,122
15	Iraq	2,008

Figure 1-2: Oil production countries, OPEC 2006

Currently, the world's oil production totals 30 billion barrels per year [2], with a current market value of 3 trillion US dollars. However, the peak of production is coming within the next decade [1], after which the production is predicted to drop precipitously. Saudi Arabia is the largest producer and proven oil reservoir in the world. Including Saudi Arabia, Middle Eastern nations hold two-thirds of the total proven oil reservoirs on earth. Although the US is a major oil production country, the US imported, on average, 8.4 million barrels/day [12] in 2012, which represents over 45% of the total domestic oil consumption. The US is also a net importer of crude oil. With an average per capita oil consumption twice the global average, the US remains heavily dependent on the Middle East to keep its economy running, as indicated in Figure 1-3. Since its peak in 2005, US importation of crude oil has dropped by at least 17% [12] due to multiple factors, including the economic meltdown, high oil prices, application of clean energy, increased domestic oil production offshore, and the decreasing price of replacing energy sources such as shale gas. Among all these factors, the application of new technology in oil exploration and production in offshore oil

reservoirs and extracting oil from previously depleted wells has made a significant contribution.

Data Source: EIA, *Petroleum & Other Liquid Fuels*, February 28, 2012, http://www.eia.gov/petroleum/data.cfm.
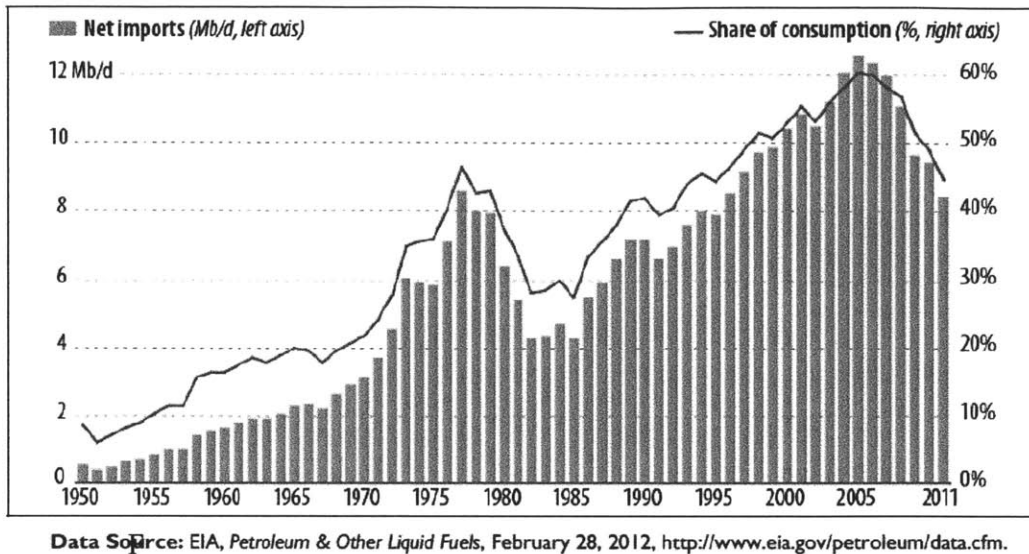
Figure 1-3: US oil import and share of domestic consumption, BP 2012

1.2 Artificial Lift Technology

1.2.1 Artificial Lift System Overview

At least 90% of current oil wells need some kind of artificial method to sustain continuous production, especially offshore wells deep under the sea floor. Ground operation has to supplement the natural reservoir pressure to sustain production[13].
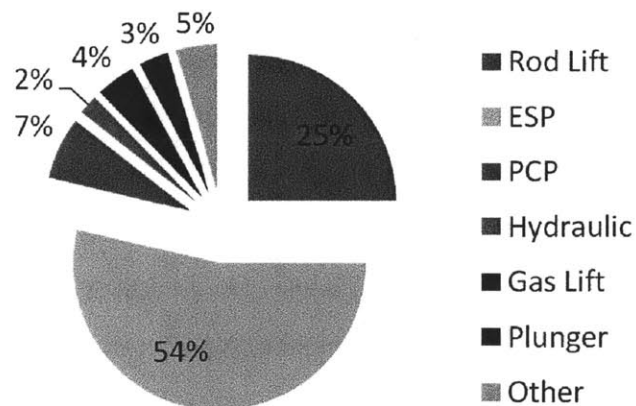
Figure 1-4: All artificial lift technologies, BP 2012

Some of the major artificial lift systems include electric submersible pump system (ESP), rod lift, progressing cavity pump systems (PCP), gas lift, plunger lift and hydraulic lift[13]. As shown in Figure 1-4, the technology most widely used, and easiest to implement on the ground, is ESP, where a pump and an electric motor are inserted downhole and add pressure to bring hydrocarbons to the ground.
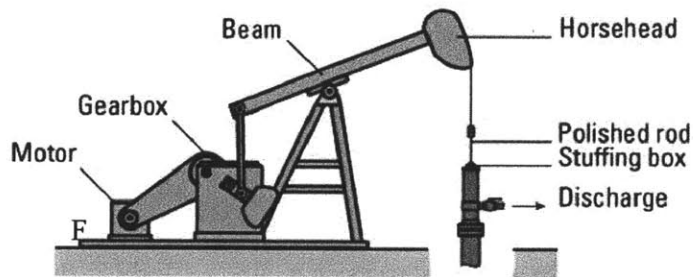
Figure 1-5: Rod lift system ground facility [32]

The rod lift system consists of the horsehead run by a motor-gear system up and down, a long cylinder barrel in the tubing and a piston-valve system at the bottom of the tubing to lift the oil up. This lifting technology has a long history and is used widely in reservoirs on the ground.

The gas lift is used widely on offshore oil rigs and is becoming a promising way to explore deep sea reservoirs because it is flexible and versatile and does not require ground wire to communicate or control. In addition, it is especially capable of dealing with the pressure, temperature, and corrosion in an undersea environment. There are over 3000 gas lift wells in the Gulf of Mexico region alone, and the number is rapidly growing.

Figure 1-6 shows how the gas lift system works. Gas is injected through a single-direction gas lift valve through a casing annulus into the main tubing, where it aerates the hydrocarbon. The oil with gas bubbles turns into a foam-like amorphous mass and flows up through the main tubing under high pressure. Ground operation can control the production speed by tuning ground valves and changing injection pressure. The injection consists of whatever gas sprays out of the reservoir,

normally methane and other natural gas, and added nitrogen from the ground. With the gas lift, no solid tubing or electric wire has to be installed in the system.
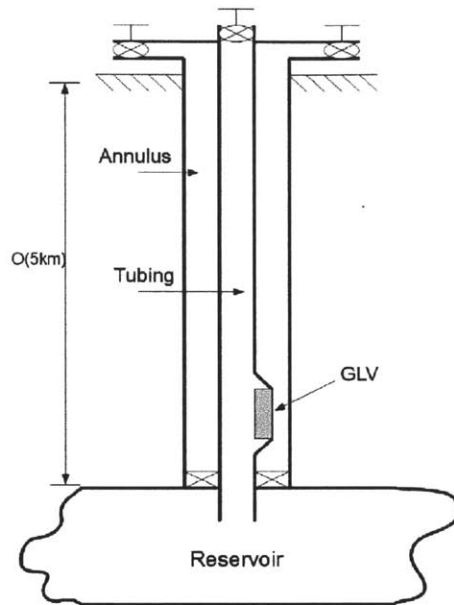
Figure 1-6: Gas lift system [3]
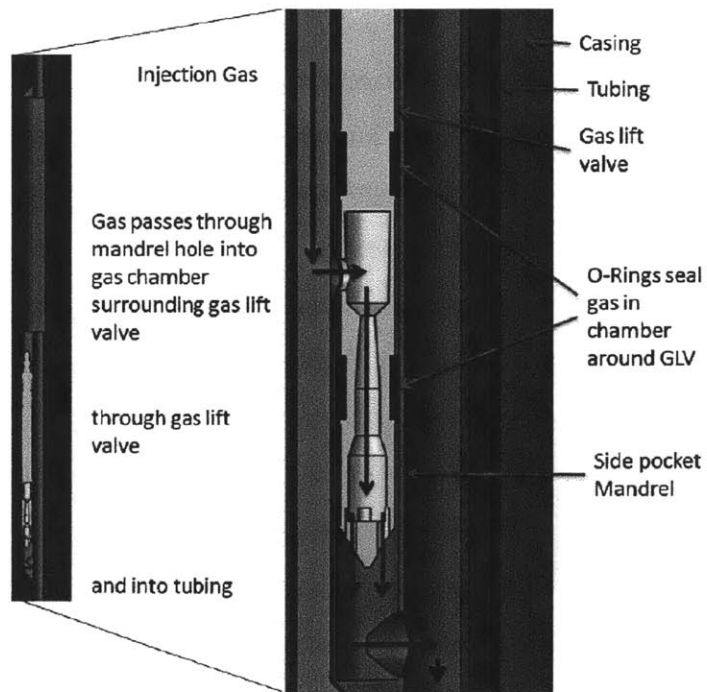
Figure 1-7: Gas lift valve[3]

1.2.2 Gas Lifting Today

The production system of gas lift wells consists of an annulus, casing and tubing. Gas is injected into the annulus through the ground valves. The gas lift valves are located in the side pocket on the main tubing called the mandrel, as shown in Figure 1-7. The valve is sealed by two O-rings at the top and two at the bottom to prevent oil or gas from flowing into the annulus. During production, high pressure gas in the annulus actuates the bellows valve and flows into the tubing. Gas mixes with crude oil and aerates it so that the low-density foam-like oil flows up through the tubing to the ground.
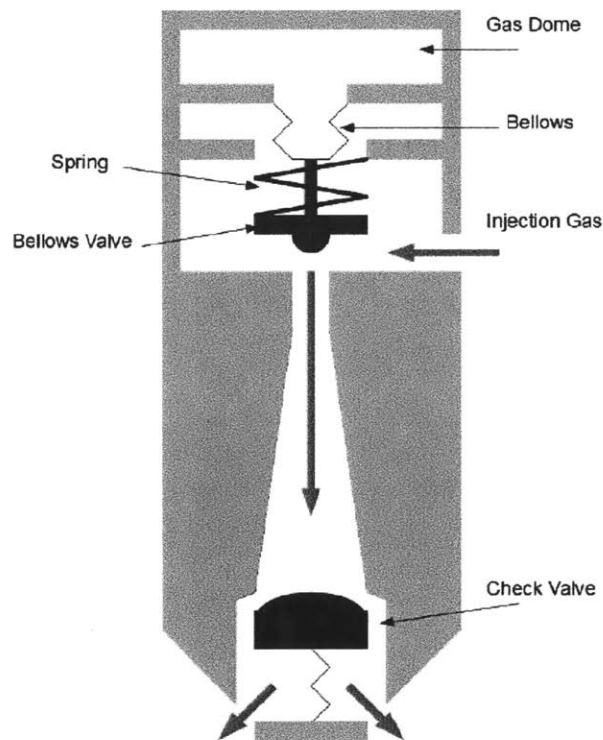
Figure 1-8   Gas lift valve cutaway [3]

The valve is the central control mechanism for the whole system and will be the focus of this thesis. It consists of a pressurized bellows and an internal check valve. When the injection gas pressure in the annulus increases beyond a certain threshold—which is designed, predetermined, and tested on the ground by changing the pressure in the bellows—the bellows will lift up to open the gas orifice. At the same time, the pressure presses on the check valve and starts the gas

17

flowing into the tubing. The major function of the check valve is to block the oil backflow regardless of its pressure; the bellows is the control mechanism to start or stop the production. As a result, the check valve is more prone than the bellows to multiple failure modes since it is in direct contact with crude oil.

Figure 1-9: Gas lift valve in market, Chevron 2009

Gas lift valves are installed with wireline operation, as depicted in Figure 1-10. During an emergency or valve failure, the valves can be retrieved with wires and repaired on the ground.

Lower to design level	Kick into mandrel	Pound to install	Shear to disconnect

Pulling tool
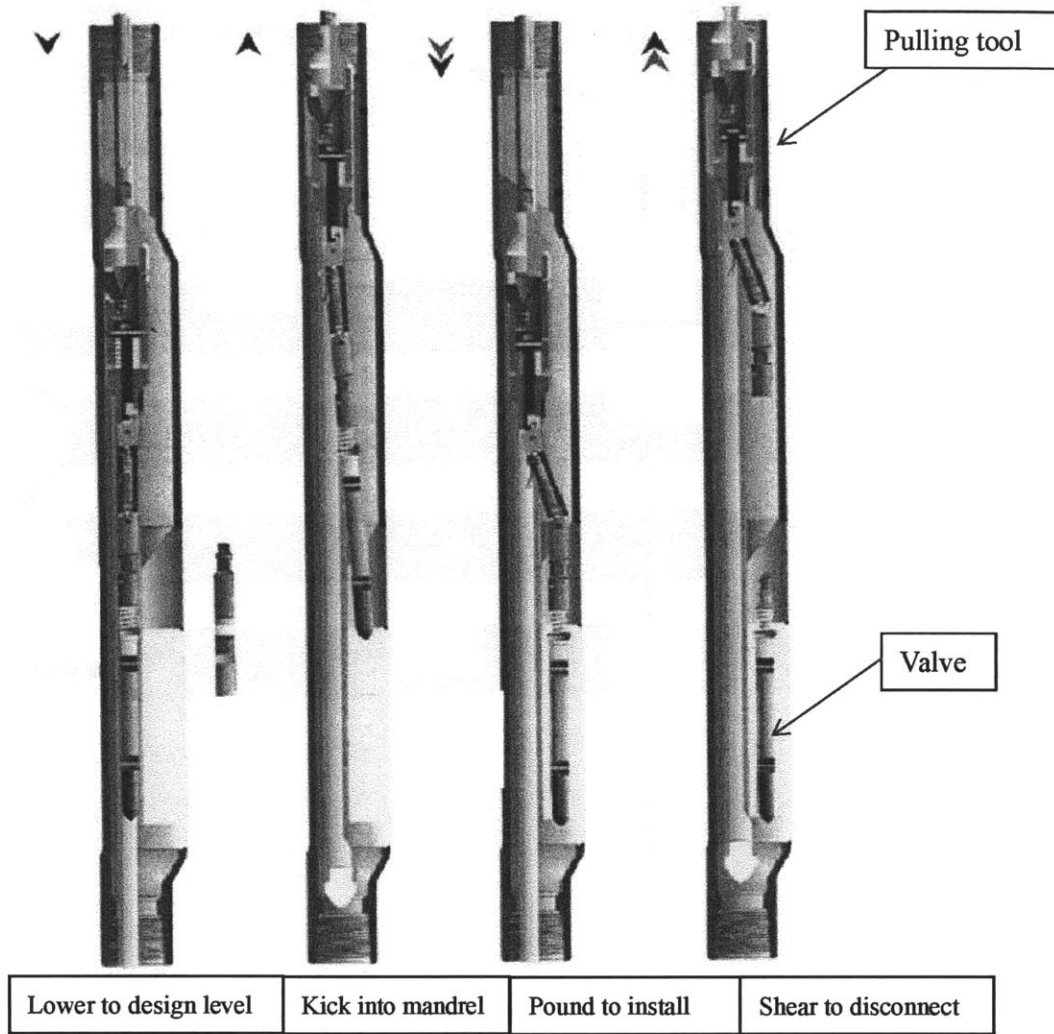
Valve

Figure: 1-10: Wireline operation [34]

Normally, one production tubing will have multiple injection points with multiple valves for different stages of production. All these valves have different actuation pressures because the tubing pressure varies for different levels. However, with the latest single point injection technology [34], the injection gas pressure could be high enough so that only one production valve is needed, at the bottom of the tubing, to achieve the whole production process.

After the drilling for a new well is finished, the annulus and tubing are normally filled with a mixture of water, gas, oil and various chemicals, which is called kill fluid. As a result, the kill fluid needs to be flushed completely out of the system to start production. This process, called unloading, is depicted in Figure 1-11. Previously, multiple production valves were also used to flush kill fluid. The valves have different actuation pressures and open one by one until no more kill fluid is available in the system. With the current technology, most wells have only two valve systems, one only for flushing kill fluid and one for production. This is the assumed design for our system so that the orifice of the production valve is never in direct contact with any liquid, even during the unloading process. Kill fluid valves only open at the beginning of the production and shut down after that. Production valves are shut down at the beginning and take over after kill fluid is gone. This process is actuated by tuning the pressure in the annulus with ground operation.

Annulus filled with liquid. Oil in tubing, not flowing. All valves are open from hydrostatic pressure. Lower unloading valves have lower bellows pressures, P1>P2>P3>P4

Gas is pumped down the annulus, flows through the top two GLVs. Liquid level in the annulus drops as fluid is pushed out of the annulus.

Injection gas pressure decreases, top GLV closes.
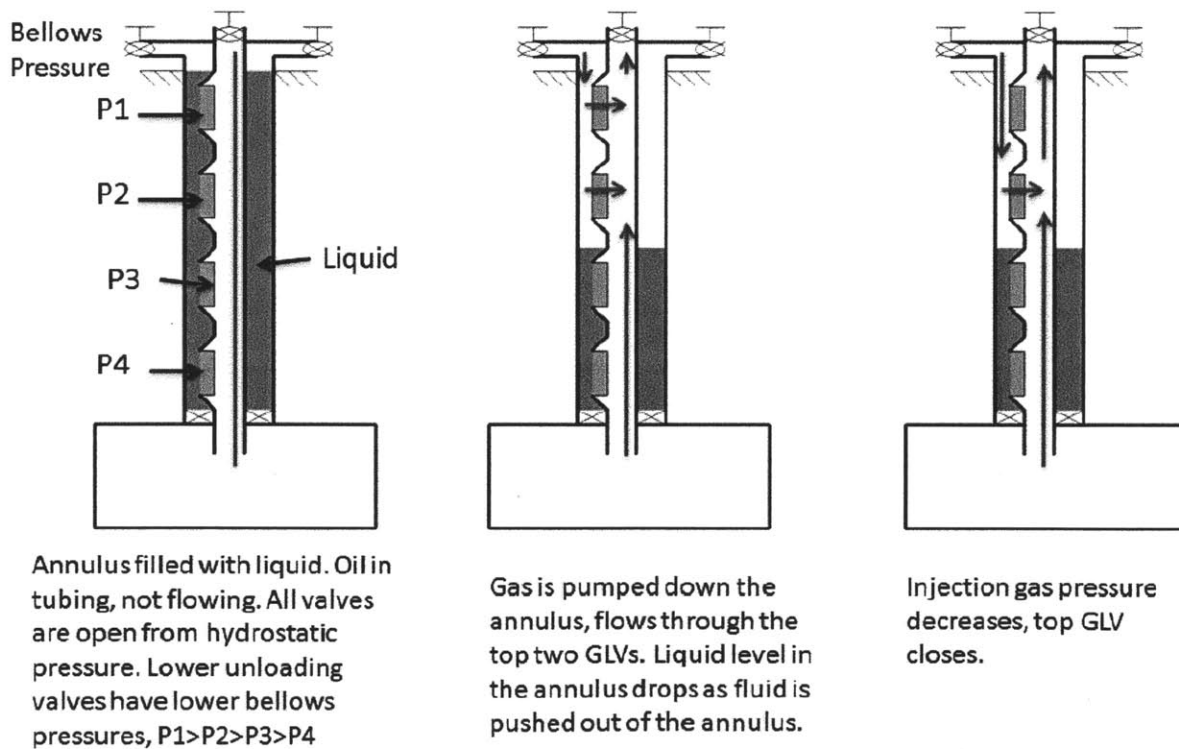
Figure 1-11: Unloading process [3]

1.3   Prior Art on Thermally-Actuated Safety Mechanism

1.3.1 Gas Lift Valve Failure Mode

By "valve failure", we mean that either the sealing of valves is compromised and the oil or gas flows back through valves into the annulus casing and even up to the ground, or that the injection is blocked and the gas injection appears to be interfered with. Valve failure can cause serious safety issues for the offshore platform, such as fires and explosions, or at least stop production.

Normal operation. Injection gas flows through the GLV and the thermal lock valve is closed.

Failure mode: debris is caught in the check valve and oil begins flowing into the annulus.

Thermal lock valve heats up and actuates, blocking flow through the orifice.
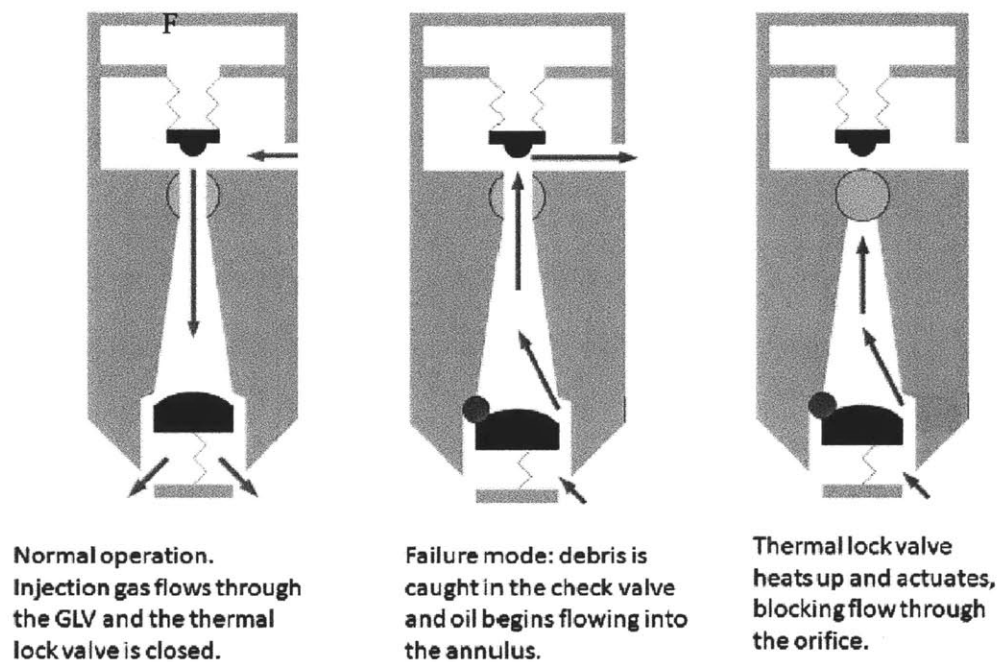
Figure 1-12: Valve failure mode and safety valve [3]

The failure modes are mostly mechanical and chemical:

● Jamming: Minerals, rocks, and large dimension solid hydrocarbons may flow through the check valve and get stuck near the perimeter, holding the check valve open regardless of the injection gas pressure, as shown in Figure 1-12.

● Corrosion: Many chemicals in crude oil are corrosive. During constant direct contact with the check valve surface, the sealing may be compromised.

21

1.3.2 Safety Mechanism

Oil production typically takes place several hundred meters below the sea floor, where the pressure is at least 3000 psi and the temperature ranges from 80°C to 100°C, in addition to the corrosive material. It is an extremely harsh production environment.

Eric Gilbertson [11] designed the first version of a thermally-actuated safety mechanism for a gas lift valve in 2011. It is the first type of safety mechanism that has a different failure mode than the original valves. Previous attempts by Schlumberger and Weatherford only added a second check valve to the system in case the first one failed. However, if the first one did fail, there was a good chance that the second would fail in the same way soon after.

Gilbertson's thermally-actuated device is an add-on device to the original gas lift valve with the pressurized bellows and check valves, so it does not change the external dimensions of the valve body. This mechanism is based on shape memory alloy contraction.
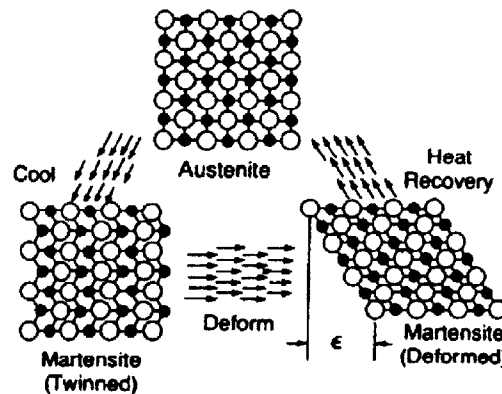
Figure 1-13: Crystal phase change [4]

The shape memory alloy is about 50% nitinol and 50% titanium. The exact ratio determines the transition temperature. When the material is heated beyond the transition temperature, it undergoes a change in its crystal form, or atomic arrangement. This change in the crystal structure in NiTi alloys is from an ordered cubic crystal form to a monoclinic crystal phase above the transition temperature[4], and there is no permanent memory for this transition. The type of transformation that occurs in shape memory alloys is known as a thermoelastic austenite transformation. It changes the material from the low temperature form, called martensite, to the

22

high temperature form, called austenite. During this process, the atomic crystal shrinks and the external volume decreases isotropically to the same level and same shape as indicated in Figure 1-13. The process is predicable and repeatable at the same temperature. The critical points in the transition are the martensite start temperature during cooling (M_s), the martensite finish temperature(M_f), the austenite start temperature during heating (A_s), and the austenite finish temperature(A_f), which are shown in Figure 1-14.
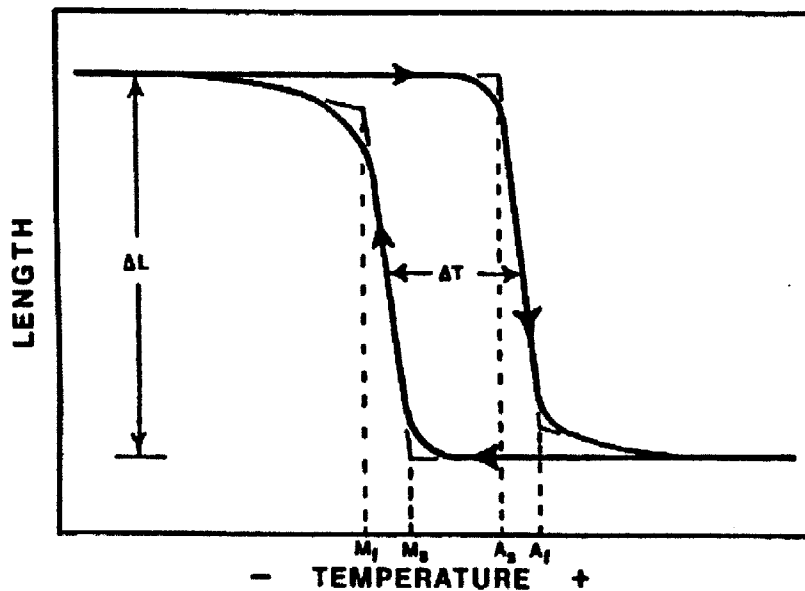
Figure 1-14: Shape memory transition [4]

The major shape memory effect on the NiTi wire is its elongation and contraction in length at different temperatures. Taking a typical Dynalloy NiTi 0.02" shape memory allow (SMA) wire as an example, the transition temperature is 70°C or 90°C depending on the specific material recipe, as shown in Figure 1-15. The contraction rate is up to 5% of the total length, and the pulling force is 3.56 Kg [11].

One handy feature of SMA wire is the adjustability of transition temperature by changing the initial tension on the wire:

$$A_s = A_o + \frac{\sigma}{M}$$

23

In this equation, σ is the initial stress on the wire and M is a constant value, 6.9 Mpa/C [11]. When A_s is increased, M_s tends to change accordingly by the same amount. Normally,two transition temperatures have a constant difference. However, we can tune either of them by changing the preloaded tension. $A_s - M_s = 20 - 30°C$
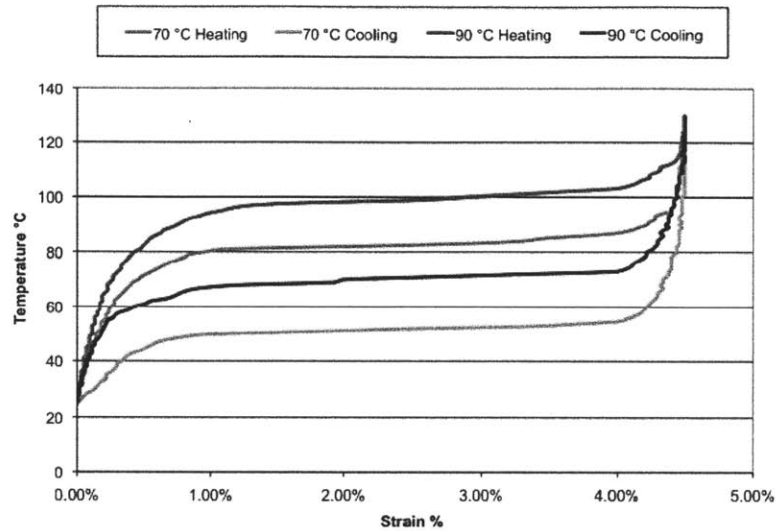
Typical Temperature vs. Strain Characteristics for Dynalloy's standard 158°F (70°C)
"LT" and 194°F (90°C) "HT" Austenite start temperature alloys, at 172 MPa

Figure 1-15: Dynalloy SMA wire data [11]
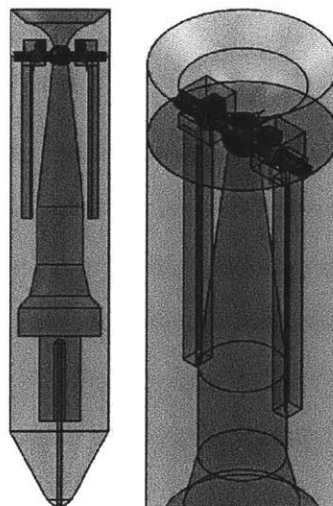
Figure 1-16:Valve body [3]

24

During typical oil production, the temperature of the valve body is in equilibrium with the annulus casing gas temperature, which is between 80°C and 100°C at deep earth level. However, during a backflow event, when the oil flows back through the valve orifice slowly and immerses the whole valve body in hot oil, the temperature can heat up beyond 100°C within a time frame of minutes. The high temperature will heat the shape memory alloy wire beyond transition temperature and lead to contraction.

As shown in Figure 1-16, this 5% contraction of the wire turns the shaft of a ball valve that was held aligned with the orifice by the torsion spring. The rotation of the shaft shuts down the ball valve and stops production. This mechanism uses the SMA wire as both a sensor to detect backflow event and an actuator to shut down the gas lift valve. This process, from backflow to complete shut down, takes up to 10 minutes and could effectively prevent further leaking.
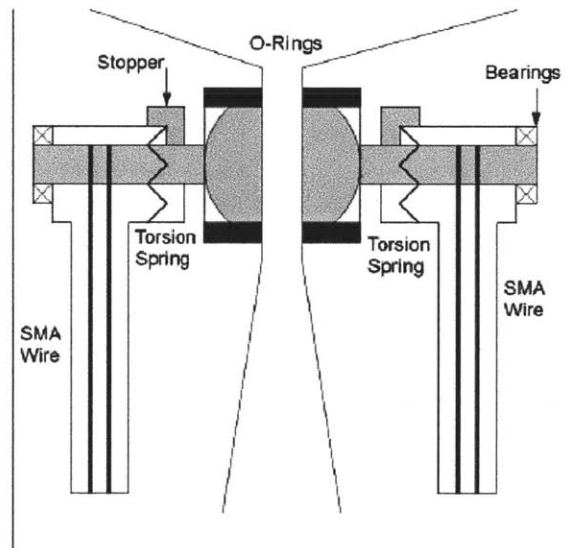
Figure 1-17: Ball valve with SMA [3]

1.3.3 Temperature Drift Technical Challenge

Our prototype has proven to be functional in a controlled environment simulating real wells. One major technical challenge to meet before it can be brought to market is production temperature drift. In real reservoirs, the downhole temperature tends to drift up and down by as

much as 1C/month due to steady pumping of relatively cold gas into the reservoir, as shown in Figure 1-17.
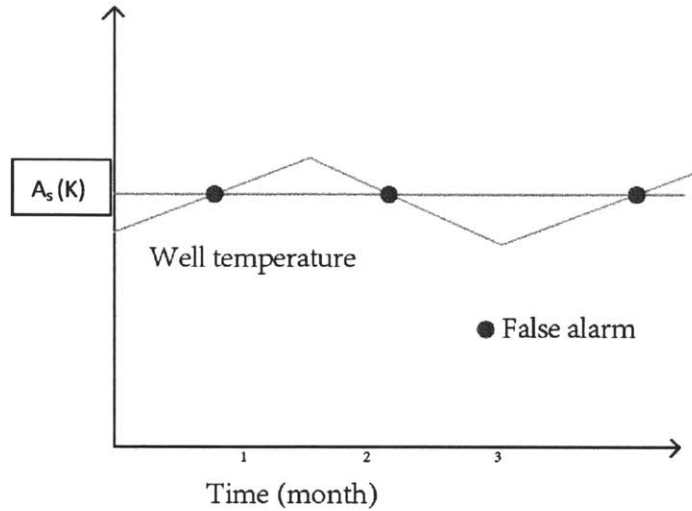
Figure 1-18: Well temperature drift

During an emergency shut-in event, when all personnel are evacuated from the platform and production is shut down due to hurricanes or other natural causes, the oil heats up the whole system slowly due to lack of cooling gas. If we use the SMA wire as a sensor and set the transition temperature to a constant value, this temperature fluctuation causes false alarms on the safety valve and shut down the valve—even if there is no backflow.

This thesis focuses on how to solve this problem, i.e. how to improve the performance of a shape memory alloy-based safety valve with normal production reservoir temperature drift.

1.4 Thesis Outline

The thesis is organized as follows:

- Chapter 1 presented the engineering challenge and prior art for this technology. The shape memory alloy technology is explained in detail with application in the thermally-actuated safety valve designed by Gilbertson *et al.* in 2011. The false alarm caused by oil reservoir temperature drift is analyzed and it's the focus for the whole thesis.

- Chapter 2 covers the possible solutions we have explored. The potential advantage and technical challenges of each are listed and analyzed.

- Chapter 3 presents the design of the electronically-controlled concept and the way to integrate it with the current gas lift valves and production tubing.

- Chapter 4 models the shape memory alloy wires with both heat transfer and structural strength. The simulation helps us understand and predict the SMA wire behavior in both air and water. Also, it helps ensure the wire's robustness under extensive tuning tension.

- Chapter 5 presents the features and requirements quantitatively of different sensors that could be implemented in the system.

- Chapter 6 documents the experiment process for testing survival performance under high pressure and temperature on both the component level and system level.

- Chapter 7 presents the system integration and functionality testing to show how the new safety valve functions in a controlled constant temperature environment.

- Chapter 8 covers the experiment on the SMA wire for multiple cycles to study its fatigue performance. A high frequency heating and cooling device was built and documented to finish such a test with over 50 cycles within a day.

This thesis ocassionally mixes metric unit and English unit for convenience.

Chapter 2
Possible Solutions & Design Space

The gas lift valve is designed to fit the current mandrels already installed in the wells. It is a huge initial investment to drill a well and install a new set of tubings. It is much easier to bring the new device to market if it can physically fit into the current valves. Moreover, the device has to survive in the high temperature, high pressure environment for up to one year, which is the average time before the old valves are retrieved, repaired, or replaced during maintenance. In addition, in terms of time frame, the reaction time requirement depends on the specific well situation and government requirement. Although the single valve price seems negligible compared to the total investment in drilling and installation of a new well, multiple valves have to be replaced regularly on each well every year. Price is definitely a factor in the design. Table 2-1 lists all the design constraints for our device.

Design Space	Constraint	Unit
Length	10	Inch
Volume	1	Inch^3
Diameter	1.5	Inch
Pressure	3000	Psi
Temperature	80-100	°C
Price	100	USD
Reaction Time	30	min

Table 2-1: Design space of safety mechanism

The dimensions are predominantly constrained by the current valve, which is 1.5 inches in diameter and 10 inches long. Considering the total volume and structural strength, we prefer to use under 1 cubic inch hollow volume in the valve body to insert the new device.

For a well 200 meters below the sea surface, 3000 psi is the minimum pressure. For our first

version of the design, the pressure target is 3000 psi, and we will try to improve the design for deep sea application with higher pressure in the following work. In terms of cost, the current single valve price ranges from 700 to 1000 USD. An additional device under 100 USD would be acceptable considering the hazard it could effectively eliminate. Ideally, the reaction should be immediate, but the initial leaking material would be oil foam and natural gas, not crude oil. Thirty minutes is an acceptable reaction time before the leaking can cause serious safety issue[17].

In section 2.2 we present some of the possible design solutions we considered (based on the above requirements) but finally rejected. They might be helpful for future researchers in this field.
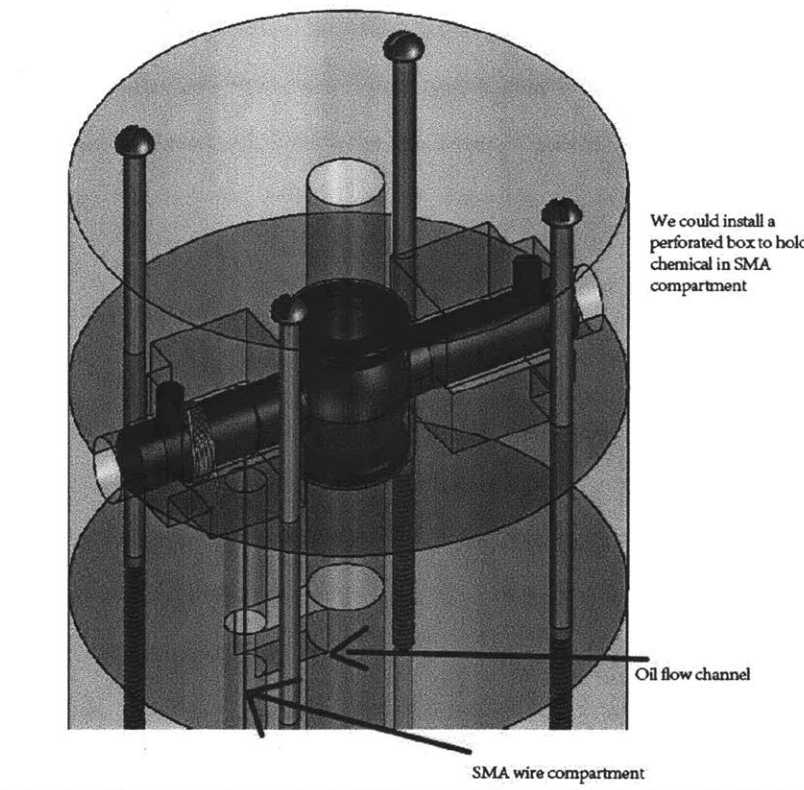
Figure 2-1: Embedded chemical case design

2.1 Chemical Heating

The chemical heating design replaces the SMA sensor in the original SMA-based design with a

29

chemical sensor. The valve orifice is connected to the SMA compartment. During a backflow event, the oil flows into the SMA compartment, where we installed a perforated case to hold the reacting chemicals surrounding the shape memory alloy wire, as shown in Figure 2-1. Oil and this highly oxidant chemical mix in the case start a fast exothermic process to release a lot of heat, warm the wire through direct conduction, actuate the SMA wire, and finally close the valve.

This chemical should be stable, stay effective for up to one year, and not decompose spontaneously under high pressure and temperature. Preferably, this chemical should be easy to handle and low in toxicity. In addition, it needs to be in solid state to fit into the perforated case.

The transition temperature has to be tuned well above the possible reservoir temperature fluctuation upper limit but below the temperature achievable through chemical reaction by adding more preloaded tension to the wire initially. As a result, no matter how vibrantly the reservoir temperature drifts, the system will not actuate unless there is oil in the orifice to react with the chemical.

Some candidates for the chemical are KmnO4, XePtF6, Na2S2O8, NaBiO3•2H2O, mostly active oxidants.
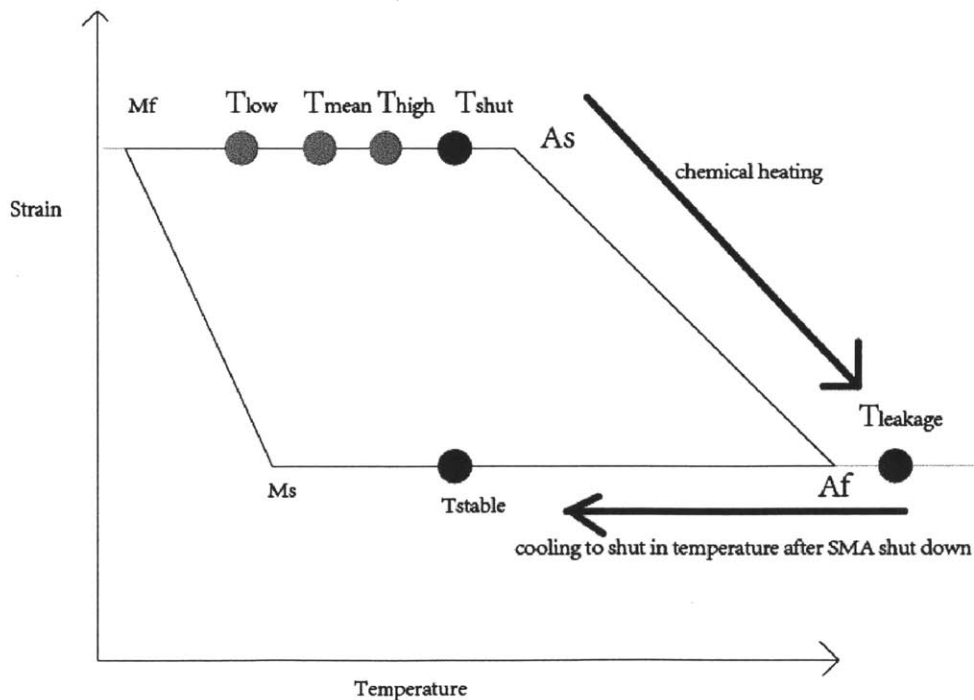
Figure 2-2: Temperature change vs. SMA wire strain

Figure 2-2 shows the temperature sequence during the whole shut-down actuation process. Tshut and Tstable are the temperatures when the cold injection gas is stopped due to maintenance or emergency natural causes. The well temperature slowly reaches equilibrium with the ambience. Tleakage is the maximum temperature of the wire during the chemical heating. The exothermic reaction will bring the wire temperature from production temperature, past A_s, the actuation temperature, and then finally past Af, the complete contraction temperature. Since there is no cooling flow, the wire will never cool down to below Ms, become martensitic, and contract again. As a result, the safety valve will stay closed.

Shut-down procedure:

1. Crude oil mixes with chemicals in the perforated case during backflow.
2. The exothermic process heats up SMA wire from Tmean (mean production temperature) to Tleakage. SMA wires finish contraction. Safety valve closes.
3. System cools back to Tstable, ambient temperature, and safety valve stays closed.
4. Whole valve is retrieved to the ground and replaced.

The major technical challenge of this solution is the chemical stability issue. All the active oxidants tend to self-decompose slowly and cannot stay effective for a fairly long time. Also, the humidity in the injection gas is an uncertainty since there is currently no drying process before injection. As a result, the chemical will increasingly absorb water, slowly react with the water, and dissolve.

Another major challenge is the coating protection on the stainless steel valve body. Since we are introducing highly active oxidant chemicals into the system with high humidity and temperature, the chemical corrosion may cause more problems than this design solves.

31
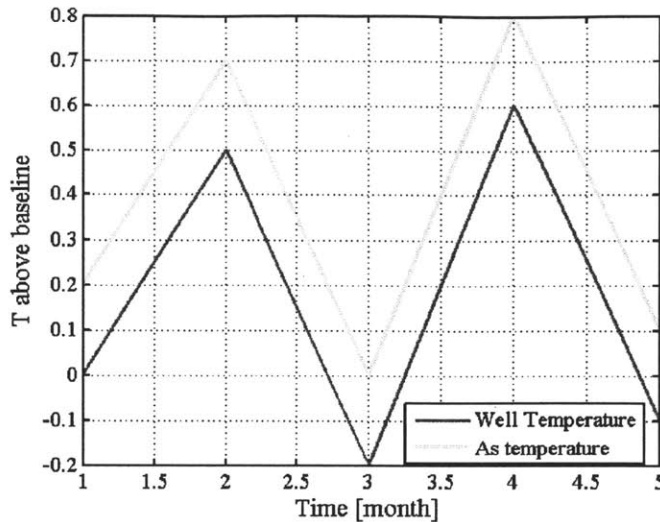
Figure 2-3: Tracking well temperature with SMA wire

2.2 Tracking Transition Temperature

2.2.1 Overall Strategy

Changing the transition temperature to track the reservoir temperature drift is another option. In short, this design seeks to change the transition temperature in the same direction by the same amount of reservoir drift to avoid a false alarm, as shown in Figure 2-3.

The major challenge of this design is incorporating a low pass filter mechanism into this tracking system, i.e. to follow the well temperature in slow frequency change to avoid a false alarm but keep the transition temperature constant during real backflow event with fast ambient temperature change to effectively actuate the system.
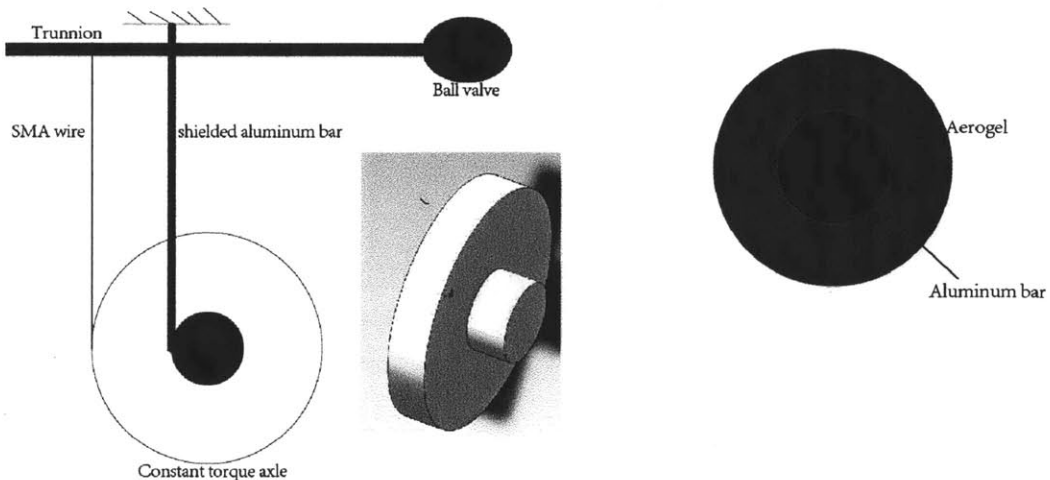
Figure 2-4: Axle mechanism to track well temperature

One of the mechanisms we designed takes advantage of the thermal expansion feature of metal. In this concept, a shielded aluminum bar and the SMA wire are connected by a constant torque axle, as shown in Figure 2-4. The aluminum is shielded with a high insulation material such as aerogel.

During slow ambient temperature change, the aluminum bar heats up, expands slowly, stretches the SMA wire by the axle, increases the wire tension, and increases the transition temperature. The reverse occurs in the cooling process. The application of the axle dramatically minimizes the length of the aluminum bar needed due to mechanical advantage. However, in the fast ambient temperature change scenario, the shielded aluminum cannot react rapidly enough in expansion to keep the A_s the same as for SMA. As a result, the ball valve mechanism can actuate as expected. The transition temperature change obeys $A_s = A_o + \frac{\sigma}{M}$ [11] where σ is the tension on the wire and M is a constant value .

2.2.2 Structural Design

We make the following assumptions:

A. Thermal expansion coefficient α is very close for aluminum and SMA at around 2×10^{-6}

B. The aluminum bar diameter is much larger than that of the SMA wire, so we can neglect the force on the axle from the SMA compared to the aluminum bar. As a result, the displacement of both SMA wires and aluminum bar are completely due to the heat expansion of the aluminum bar.

The design has a general goal of keeping the A_s, the transition temperature, change the same with the ambient temperature change ΔT by tuning the tension on the SMA wire. As a result, the SMA wire can avoid phase change due to ambient temperature drift.

$$\Delta A_s = \Delta T \tag{2.1}$$

The transition temperature change follows the rule

$$A_s = A_o + \frac{\sigma}{M} \tag{2.2}$$

where M = 6.9 Mpa/C [4] is a constant value. After combining these two equations, we have the expected relation between wire tension and ambient temperature change

$$\Delta T = \frac{\sigma}{M} . \tag{2.3}$$

We also know the heat expansion of the aluminum bar follows the rule

$$\varepsilon = \frac{\Delta z}{L} = \alpha \Delta T \tag{2.4}$$

where α is the thermal expansion coefficient and ε is the strain,

After we plug in the strain-stress relation of

$$\sigma = \varepsilon \cdot E \tag{2.5}$$

, where E is the Young's modulus, with Equations 2.3 and 2.4, we have the relation between aluminum bar strain and SMA wire strain

$$\varepsilon_{alum} = \alpha \cdot \varepsilon_{sma} \cdot E_{sma} / M . \tag{2.6}$$

We then express the total SMA wire strain ε_{sma} as the ratio between real expansion caused by aluminum bar stretching $N\Delta z$ substracted by the expansion due to the heat expansion of SMA wire itself, and the total length of SMA wire. Δz is the expansion of the aluminum bar and N is the axle diameter ratio.

$$\varepsilon_{sma} = (N\Delta z - \alpha \cdot \Delta T \cdot L_{sma}) / L_{sma} \tag{2.7}$$

We then plug equation 2.7 in equation 2.6 and get the relation between the length of the two materials

$$\varepsilon_{alum} = \alpha \frac{N\Delta z - \alpha \cdot Lsma \cdot \Delta T}{Lsma \cdot M} E_{sma} \tag{2.8}$$

Therefore, in equation 2.8 we replace the strain for aluminum bar ε_{alum} with the ratio of its expansion and total length and express ΔT with Δz in heat expansion Equation 2.4. Finally, we cancel out Δz on both sides of the equation and get the ratio between two materials as

$$\frac{L(alum)}{L(sma)} = \frac{M}{\alpha \cdot M} \cdot \frac{1 + \frac{\alpha \cdot E(sma)}{M}}{N} \tag{2.9}$$

Plug in the values for the constants of M and E=7.5e10 Pa to collect the numerical ratio between two materials as

$$Ratio = \frac{L(alum)}{L(sma)} = \frac{5.5}{N}$$

where N is the ratio between the larger raduis and the smaller one on the axle, i.e. SMA/Aluminum.

This is the required ratio between two wires to ensure that the transition temperature can keep a constant difference above the ambient temperature, as required (see Figure 2-3). For a

typical gas lift valve, the overall maximum length is less than 10 inches. If we install a 10-inch-long aluminum bar, the maximum SMA wire length turns out to be 1.8 inches. A single wire of this length would not have enough contraction length to pull the ball valve completely. Another axle or lever system would be needed at the wire-valve joint.

2.2.3   Thermal Design

The insulation design of the aluminum bar determines the valve closure timing. We choose aluminum because of its relatively high thermal expansion coefficient (among cheap metals), ease of manufacture and large enough Young's modulus. We want to model the aluminum bar heat transfer and predict the closure behavior with different dimensions of the bar and insulation layer. The major heat transfer mode is direct conduction from the stainless steel casing to the aerogel and from the aerogel to the aluminum bar. In our case, the cross section of aluminum bar has a very large Biot number; therefore, we can neglect the temperature difference within the metal.

The dominant thermal resistor turns out to be the aerogel insulation layer compared with the small contact resistance between steel casing and aerogel and between aerogel and aluminum.
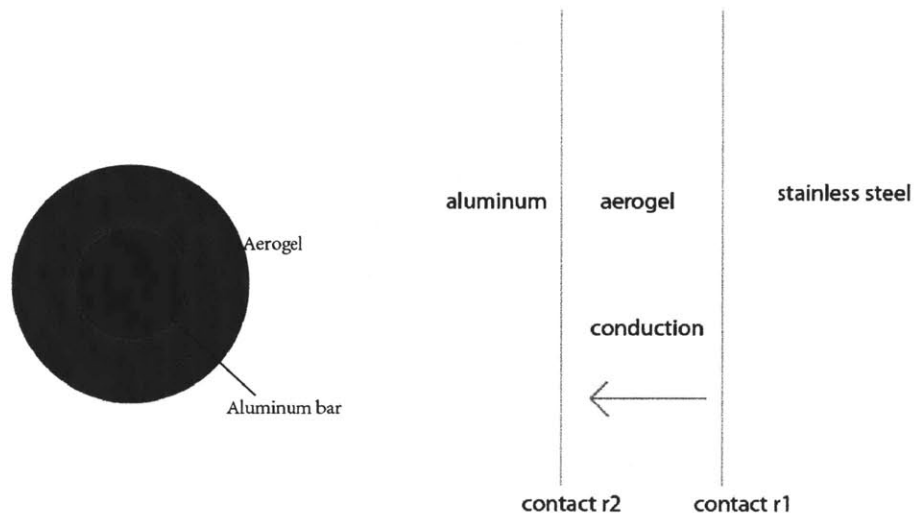
Figure 2-5: Insulated aluminum bar and equivalent thermal resistors

We assume that the aerogel outer surface temperatures are in equilibrium with the metal in

contact, stainless steel and aluminum, respectively. The stainless steel temperature represents the ambient temperature in the well. We neglect the contact thermal resistance r_1 and r_2 in this analysis. Therefore, we can focus on the heat transfer through the aerogel.

This is effectively conduction and follows the conduction rule

$$q'' = -KA \cdot \frac{\Delta T}{\Delta x} = -2\pi r L \cdot \frac{K\Delta T}{\Delta r} \tag{2.10}$$

with a small variation for aerogel cylinder. K is the conduction transfer rate, A is the heat transfer contact surface area and r, L are the dimensions of the cylinder. We then introduce the idea of equivalent thermal resistor

$$R = -\frac{\Delta T}{q''} . \tag{2.11}$$

Therefore, the infinitesmal thermal resistor for a smal thickness within the cylinder is

$$\Delta R = \frac{\Delta r}{2\pi r l K} . \tag{2.12}$$

We can calculate the total thermal resistor by taking the sum of all these infinitesmal resistors

$$\sum \Delta R = \frac{1}{2\pi L K} \ln(\frac{r(out)}{r(in)}) \tag{2.13}$$

Where r_{out} and r_{in} are the outer and inner radii of the cylinder.

The ambient temperature keeps rising from initial temperature T_o at a speed of 1C/month and the temperature at time t in seconds can be expressed as

$$T_{out} = T_o + \frac{t}{30 \times 24 \times 3600} . \tag{2.14}$$

Then we plug 2.15 in the heat conduction equation with transient temperature T_{out}, aluminum bar temperature rise $\Delta T + T_o$ and the total equivalent thermal resistor R to obtain the instant heat transfer rate at time t

$$q'' = (\frac{t}{1\,month} - \Delta T) \cdot \frac{1}{R} . \tag{2.15}$$

At the end, with the sum of instant heat transfer , the total heat transfer results in a temperature rise at the aluminum bar

$$\int_0^t q'' dt = C_{alum} \cdot M_{alum} \cdot \Delta T . \tag{2.16}$$

After we take the derivative with respect to time on both sides of 2.17, we have an ordinary differential equation in terms of ΔT. We can then solve this equation by plugging in the boundary condition of $\Delta T(0) = 0$, $\Delta T(1\,month) = 1$, the constant values K = 0.02W/m.K for aerogel ,C_{alum} = 910 J/K.Kg, ρ_{alum} = 2700 Kg/m^3 , K_{alum} = 150 W/m.K. The temperature rise of aluminum bar

follows the following equation and definitions

$$\Delta T = \frac{A}{1\ month} \cdot e^{-\frac{t}{A}} + \frac{1}{1\ month}\ (t\text{-}A), \quad A = 38880\ \ln(\frac{r(out)}{r(in)}).\qquad (2.17)$$

We can see from equations above that the temperature fluctuation of the aluminum bar is a function of both the dimensions of insulation design, i.e. the aerogel outer diameter and the bar outer diameter, and the environment temperature change rate. We conduct a case study on one of the feasible designs within the design space to see how the closure behavior is affected by the thermal design.

Design example: $\qquad \Delta As = \Delta T$

$\quad$ D$_{aerogel}$ $\quad=\quad$ 0.5 inch $\qquad$ (max acceptable diameter) $\qquad$ D$_{alum}$ = 6 mm

$\quad$ with A$_s$-T$_{well}$ = 0.3K $\qquad$ actuate time = 6.8 min $\qquad$ at 5C/hour
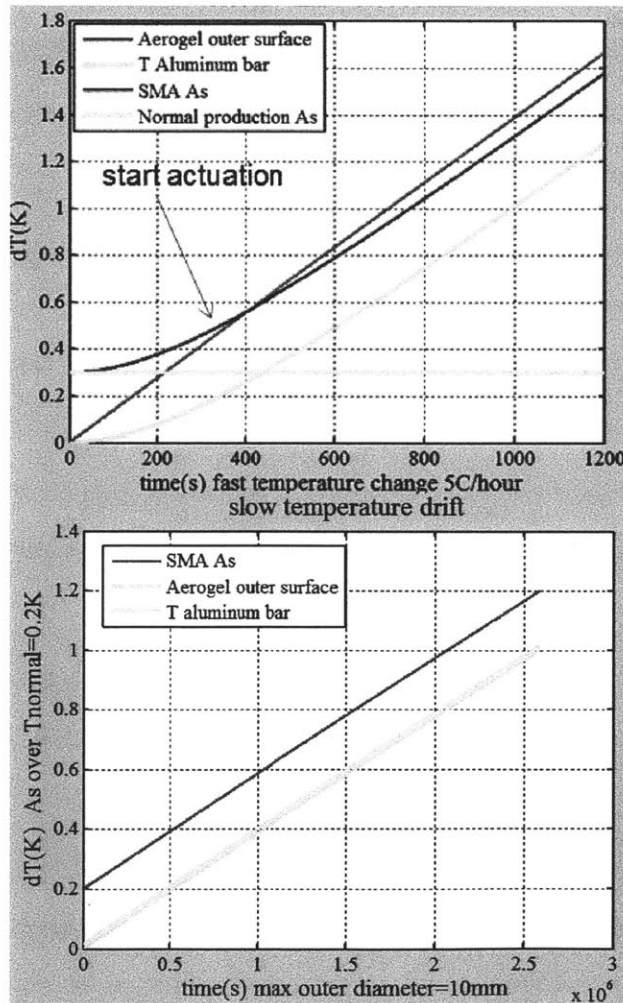
Figure 2-6: Thermal simulation in fast and slow temperature change scenarios

37

With this structural and thermal design, the change in transition temperature on the SMA equals the temperature change on the aluminum bar. In the fast response case, when the well temperature (aerogel outer surface temperature) rises rapidly and the transition temperature cannot keep up due to the insulation effect, the safety mechanism will start to actuate when these two curves cross, after about seven minutes. With a slow well change, the transition temperature keeps rising by the same amount with the ambient environment and avoids a false alarm.

Our repetitive tuning of the dimensions of the insulation and aluminum bar shows that the closure timing does not have a linear relation with either the insulation or the bar dimension. Their effects are coupled. Thus, we can not minimize the closure time by maximizing the aerogel thickness. Although more insulation would decrease the heat transfer to the aluminum, a smaller metal bar due to the expanding insulation would also need a smaller amount of heat to expand, and thus delay the closure. In contrast, the slow temperature tracking behavior is not sensitive to change in insulation dimensions.

Shut down procedure:

1. SMA wire transition temperature stays above ambient temperature with a constant value during normal production.
2. During backflow the fast heating, A_s curve intercepts the ambient temperature curve and the safety valve starts to close.
3. System cools back to Tstable, ambient temperature, and the safety valve stays closed.
4. The whole valve is retrieved to the ground and replaced.
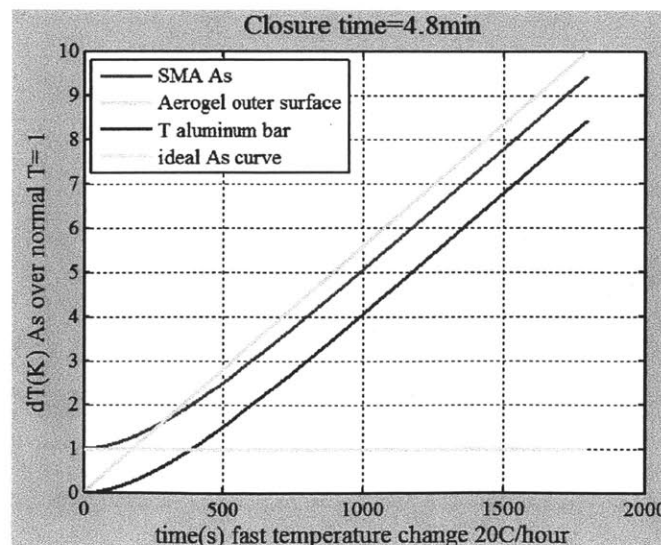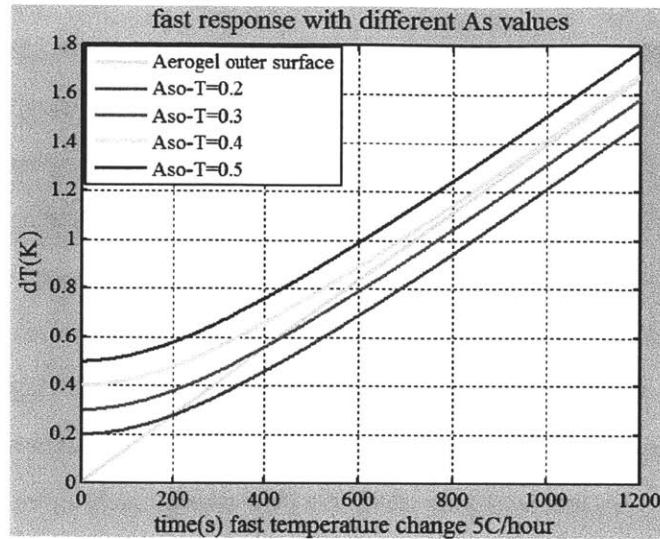
Figure 2-7: Thermal simulation with different A_{so} values and ambient change rates

As shown in Figure 2-7, in different cases with different predetermined As, the valve SMA will actuate at different times. With a too large A_s vs. T_{well} difference, the well temperature and A_s curves might never cross and then never actuate. We have to choose the preset As value carefully to ensure reliability. Also, the system is also sensitive to the change rate of the well temperature. A large A_s vs. T_{well} SMA wire will effectively actuate with a 20C/hour well temperature change but will not be functional in the 5C/hour case.

One major flaw in this design is the reliability of complete closure. When the SMA As and ambient temperature curves intercept, the valve starts to contract. As the ambient temperature increases, the valve As and Af temperatures increase accordingly. It is highly likely that the A_f is too high and the wire will never finish complete contraction, i.e. completely close the valve.

This temperature tracking mechanism is less prone to corrosion, high pressure, and high temperature damage since all the parts are mechanical. However, it takes special tuning of the preloaded SMA tension to fit each well since the well temperature various greatly from well to well. It takes a long time to actuate after the backflow initially appears because the oil has to heat up the stainless steel valve body first, before heating up the embedded safety mechanism parts. Everything has to fit together and work perfectly to shut down the production valve as expected.

2.3 Chapter summary

We explained the two possible design concepts to solve the false alarm problem caused by temperature drift. The advantages and disadvantages for both designs are discussed. The ground work of mathematical modeling and design is presented. Future researchers can follow the path and explore deeper in these directions.

Chapter 3
Electronically-Actuated Safety Mechanism

The overall strategy behind this concept of solving the temperature drift problem is to replace the shape memory alloy with a sensor-microprocessor circuit and preset the transition temperature well above the possible reservoir temperature drift range to avoid a false alarm and be able to actuate at the same time. Also, thermal heating from the ambience is replaced with electrical heating from a battery-supercapacitor energy storage system. With controlled voltage and current, the actuation behavior is more predictable and reliable. The rest of the thermally-actuated safety mechanism stays the same, including the ball valve design and the shape memory alloy mounting. This new concept is an improvement of, and an add-on device to, the original version.
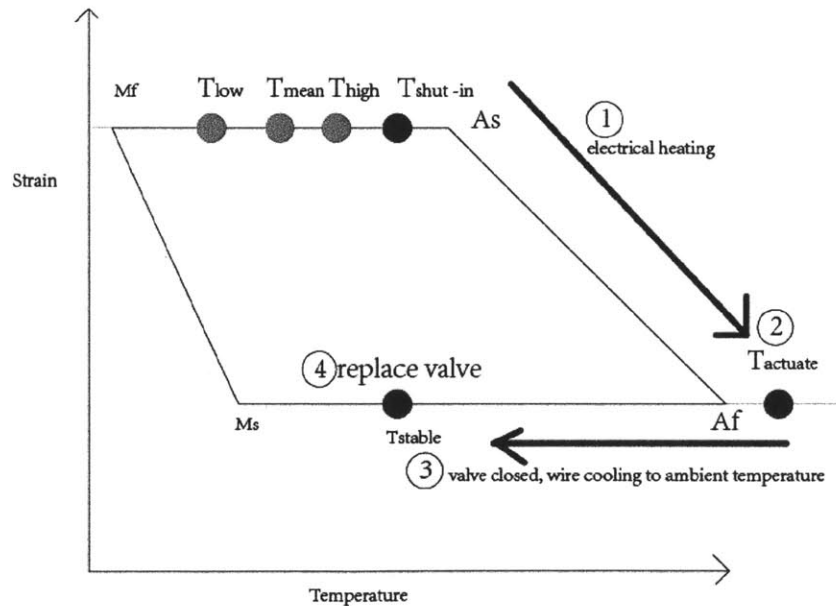
Figure 3-1: Temperature strategy in electrical heating

We have to avoid the possibility of false alarms during shut-in as well. The transition temperature should be well above $T_{shut-in}$, which is the system temperature when production is shut

down due to maintenance or weather issues and the temperature rises to ambient temperature due to the lack of cooling gas. This temperature is normally above the well temperature drift range.

This circuit should be also able to store and pass energy to the shape memory alloy to actuate contraction. After the actuation, the wire reaches a maximum temperature $T_{actuate}$, and slowly cools down to the ambient temperature, which is still well above M_s. As a result, the wire will maintain its contracted length. The valve could be retrieved to the ground for repair and replacement soon after.
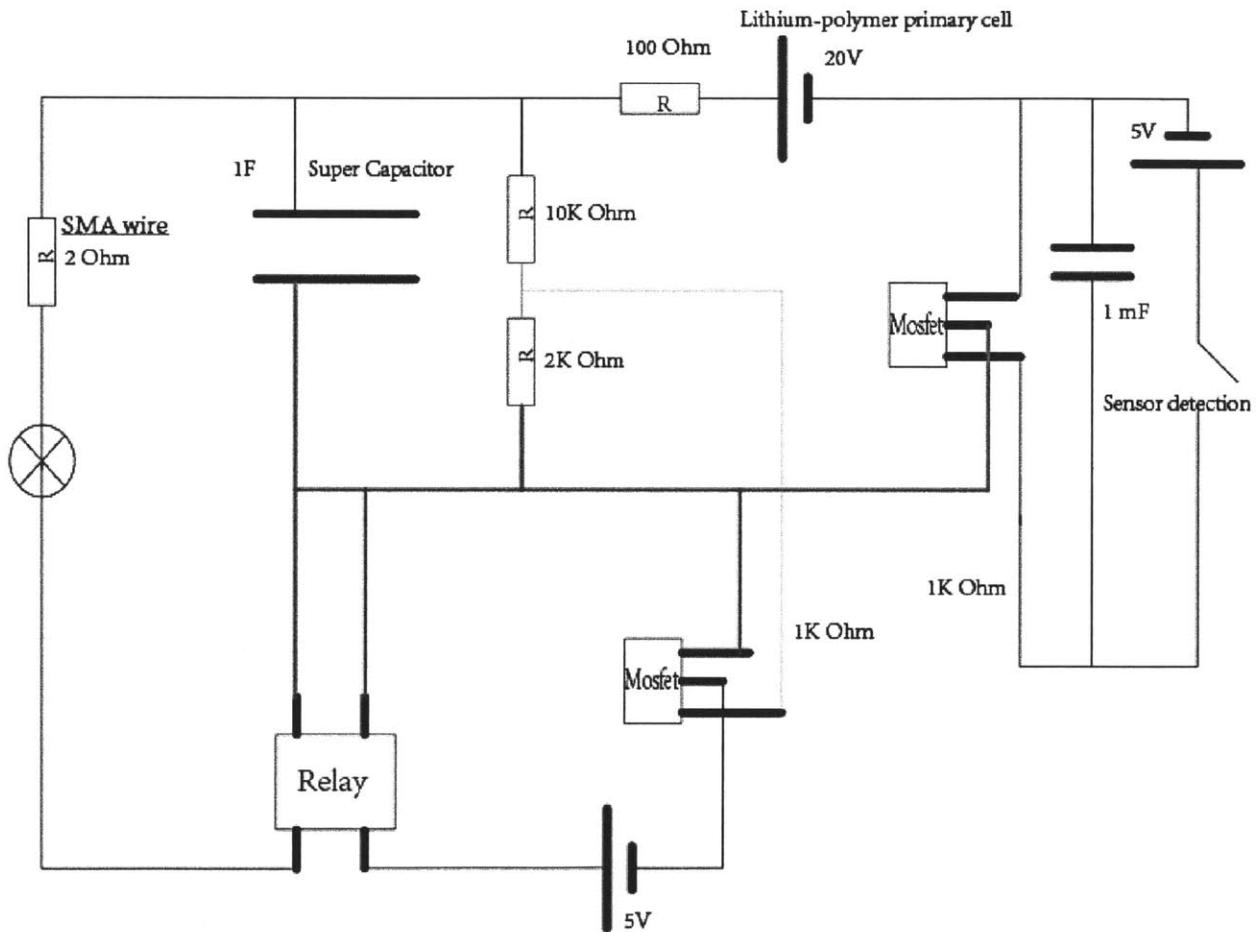
Figure 3-2:   Control circuit schematics

3.1 Control Circuit Design

3.1.1 Circuit

Figure 3-2 shows how the passive control circuit works. By " passive," we mean it is not

consuming any energy before there is a backflow event. The imbedded conductivity sensor system

monitors the situation in the gas lift valve orifice. Once there is crude oil, water, or aerated oil

foam in the orifice, this dramatically changes the resistance between the sensor probes. The circuit

is immediately closed. The first 5V battery will apply a voltage charge on the first MOSFET to

close the charging circuit. The energy storage lithium battery will start to slowly charge the

supercapacitor with a physical discharge limit of 200 mA, which takes up to 3 minutes in

experiments. The voltage divider on the supercapacitor monitors the voltage constantly. As soon

as the voltage reaches the designated value, it will apply enough voltage to the second MOSFET

to close the actuation circuit, which in turn applies enough voltage to the relay to start the fast

discharge from the supercapacitor to the shape memory alloy. The discharge is finished within 1

second. As soon as the wire is hot enough, it will finish the 5% contraction and close the valve. In

the downhole environment, it is never going to cool to below the Ms value and keep the valve

closed. The whole process takes up to 3 minutes.

The passive sensing system is based on a simplified version of the conductivity sensor. The

metal plate electrodes are installed on opposite sides of the flow orifice. The sensor is in series

with the lithium 5V battery and the first control MOSFET. During normal conditions, only

injection gas goes through the sensor and the resistance is extremely high. When oil foam flows up

through the orifice, the low resistance material closes the circuit and applies the voltage on the

MOSFET to actuate the following procedures.

The circuit consists of two major functions: energy storage and sensing. The reason for

including the dual battery-capacitor system is the life range requirement and the memory alloy

contraction current requirement.

It takes 4A for at least 1 second [11] to complete the 5% contraction for the 0.02-inch diameter

SMA wire we use. However, the lithium ion battery has a maximum 200 mA discharge rate with

100 Ohm resistance [15] due to its chemical mechanism. It is a perfect energy storage device due

to the low self-discharge rate of 2% per year [15] but it is less than ideal for actuation current. On

the other hand, a supercapacitor can hold up a large amount of energy with a high capacitance, and

the discharge rate is technically unlimited [7]. The only drawback is the high self-discharge rate of up to 30% per day. As a result, we decide to combine these two types of energy storage devices to store the energy for up to a year during normal operation and discharge the energy quickly through capacitors in actuation. Turner and Xu have designed such a circuit [8][9] for other purposes, especially in power plant and electronic appliance energy regulation. Our version is an improvement to and modification of their design. Our circuit design has to store and deliver a much larger amount of energy and has to survive in a harsh environment for extensive periods of time. Also, our electronic system is the first one to be integrated with gas lift oil production systems.
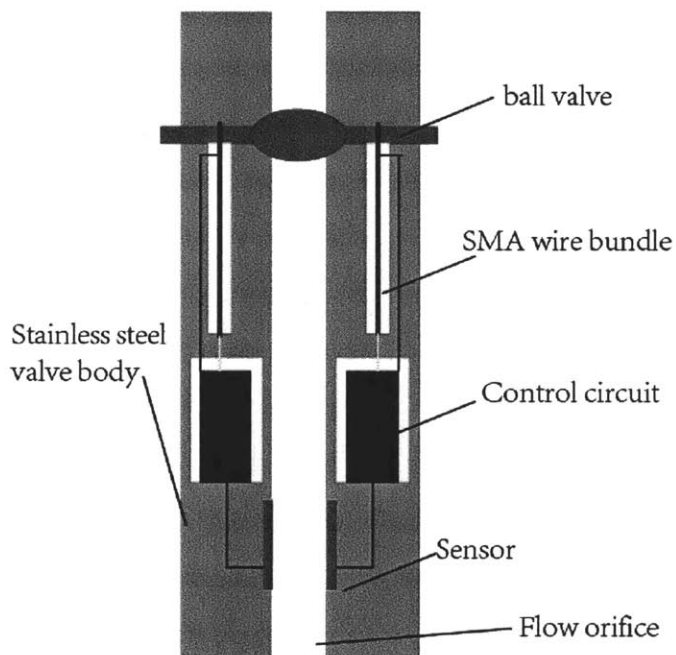
Figure 3-3: Valve body with integrated circuit system
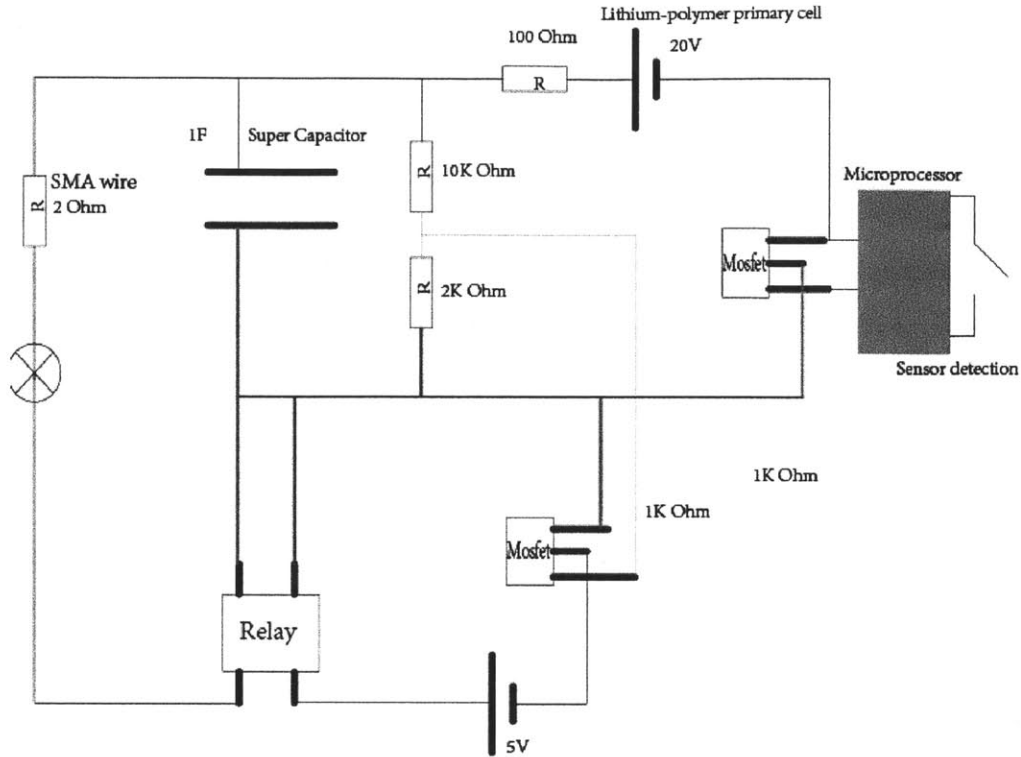
Figure 3-4: Control circuit with embedded microprocessor

A more advanced version includes a high pressure, high temperature microprocessor to replace the passive control system. The sensor system shown in Figure 3-4 sends real-time data to the microprocessor, which records and analyzes the turbidity, pressure, temperature, and conductivity data in the orifice, makes decisions about when to start the shut-down process, applies a predesigned voltage to the MOSFET of the energy storage system, and starts the process. In this version, the processor and sensor are constantly consuming energy to execute the monitoring task.

To save energy, the system could be turned on every 24 hours or even every week to collect data. With the current technology, a low power sensor consumes as little as 1 mW and can run on the lithium button battery for up to 20 years. In addition, with the microprocessor, the noisy data from the sensor can be filtered, stored, compared and even sent back to the ground. We discuss how to analyze raw sensor data and use the information to make decisions in Chapter 5, Sensor Selection.
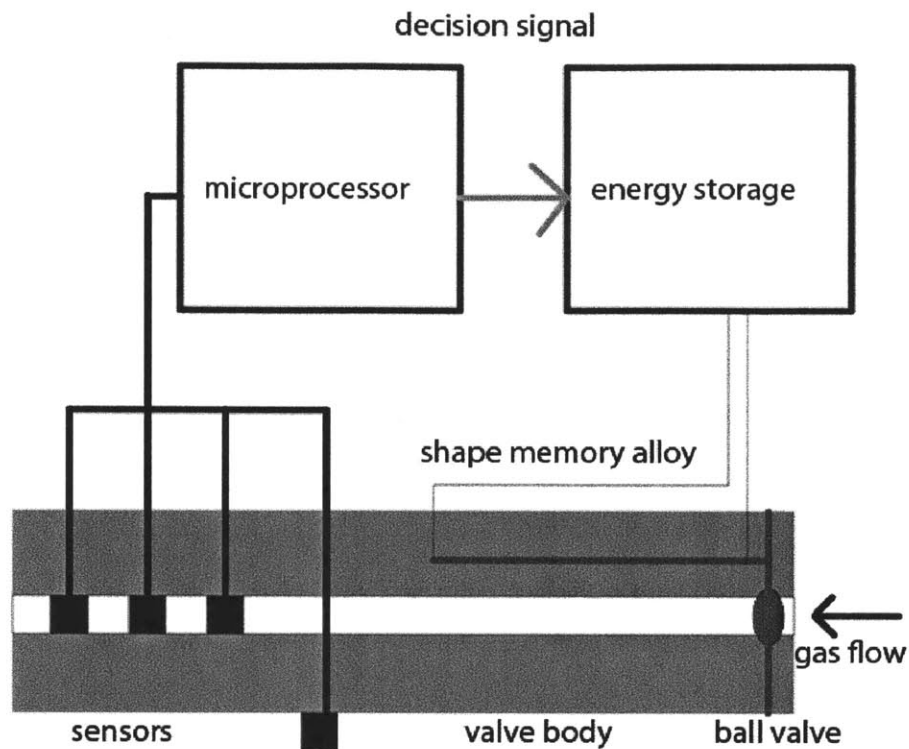
Figure 3-5: Remote control version

As shown in Figure 3-5, the microprocessor collects data from multiple sensors (turbidity, conductivity, temperature) in the flow orifice, makes decisions based on the data, and sends a decision signal to actuate the energy storage circuit to start our shape memory alloy mechanism to shut down the production valve.

A variation of the active smart version shown in Figure 3-5 includes a pressure sensor. This sensor is attached to the valve body in direct contact with the annulus casing gas. By tuning the high pressure valves to change the pressure in the annulus casing in a predetermined pattern, the ground can send a command signal to the microprocessors. With this sensor, we can send pressure signals from the ground to remotely control the behavior of the safety valve without a wire. It is even possible to design a pressure-based language with different patterns of pressure fluctuation to tell the microprocessor to make different decisions, e.g. hold valves open for one hour during

special maintenance and unloading, close the valve although no abnormal change of sensor data is found, calibrate the sensor and reset the current value to zero, etc. Figure 3-6 illustrates one possible way to send different command by changing the duty ratio with PWM signal.
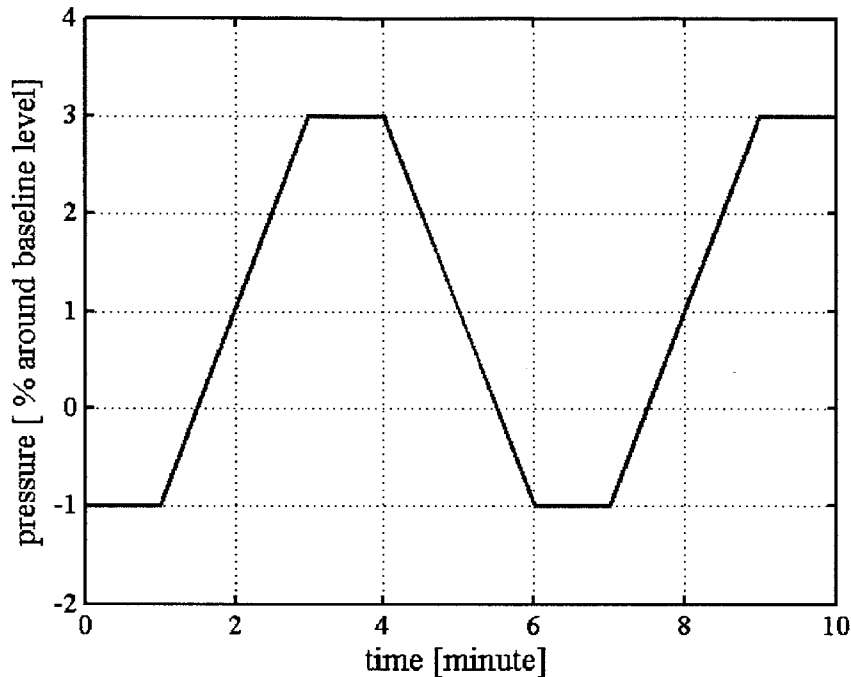
Figure 3-6: Sample pressure wave form in annulus casing

$$\text{where} \quad \text{Duty ratio} = \frac{High\ period}{High\ period + Low\ period}$$

According to Chevron [17], the annulus casing pressure can vary with a maximum frequency of 30%/minute by tuning the CHOKE (ground gas injection valve) on the ground. Therefore, by changing the duty ratio of the pressure wave form, the signal can instruct the microprocessor to make different decisions. Although it is only a one-direction communication, the gas lift valve is much smarter with this remote control mechanism.

3.2 Part Selection

We built a 3x large scale prototype [3]. Two 0.02" diameter SMA wires actuate the ball valve, each of which is 5 inch long [3] to get 36N force to pull the ball valve. The design goal is to store enough energy to pass 4 amps of current for at least 1 second [11] through each of the wires

during actuation. We discuss below how to select the appropriate electronic parts for this prototype.
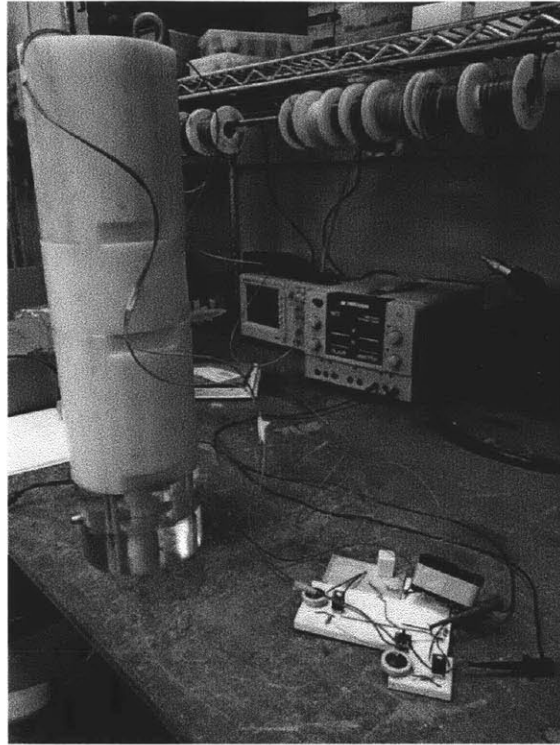
Figure 3-7: 3X large scale polyethylene prototype

The major parts of this circuit include battery, MOSFET, supercapacitor and relay. Each has to satisfy the pressure and temperature requirements and also has to have enough energy capacity. Major energy deliver processes are charging, during which the battery charges up the supercapacitor slowly, and discharging, during which the supercapacitor dumps a large current through the SMA wire.

Battery

A lithium battery can survive in a high pressure environment with a temperature up to $80°C$. High temperature testing up to $150°C$ caused an explosion and fire in the oven. Further work needs to be done to improve performance or find a better type of battery. The battery should have enough energy for the whole process of wire heating, and also enough voltage to confine the charging stage to a reasonable period of time. We also considered other options, such as an

alkaline battery, which has an extremely low self-discharge rate and can stay functional for up to ten years, but the discharge rate is too low for our purpose. As a result, the alkaline battery system would have a very long charging stage before actuation.

The energy requirement is calculated based on total consumption on the shape memory alloy wire. With a constant current through the wire, the total energy dissipation follows the Joule's law

$$E = I^2 \cdot Rt .$$
(3.1)

However, the total energy dissipation should include the energy lost due to the battery internal resistance

$$E_{total} = E_{loss} + E.$$
(3.2)

By plugging in the data   I=4A, t=1s and the resistance of the wire R_{wire} in 3.3,

$$R_{wire} = 0.22 \text{ Ohm/in x5 inch} = 1.1 \text{ Ohm } [11]$$
(3.3)

we know the total energy dissipation should be around 100J. With a safety factor of 2, the total energy we need to store in the battery should be

$$E_{total} = 200 \text{ J}.$$
(3.4)

In conclusion, the battery capacity requirement is 200J with a design voltage we will discuss later in this chapter. A lithium battery has a natural current limit, a natural power limit of 340 W/kg [33], and an energy density of 500 W.h/L. With our mechanical volume limit and the electrical features of the off-the-shelf button cells, the output current limit is generally 200 mA. This output current performance can constrain the charging stage to several minutes.

Supercapacitor

Electrical double-layer capacitors (EDLC) are, together with pseudocapacitors, part of a new type of electrochemical capacitors called supercapacitors, also known as ultracapacitors. Supercapacitors do not have a conventional solid dielectric. Rather than two separate plates separated by an intervening insulator, these capacitors use virtual plates made of two layers of the same substrate. Their electrochemical properties, an "electrical double layer," result in the effective separation of the charge despite the vanishingly thin (on the order of nanometers) physical separation of the layers. The lack of a need for a bulky layer of dielectric (and the porosity of the material used) permits the packing of plates with much larger surface area into a given volume, resulting in high capacitance in uniquely small packages. The capacitor for our

49

design should have large enough capacitance to hold enough energy to heat up the SMA wire, but also not too much capacitance to confine the charging and discharging within a reasonable period of time. Also, compared to a constant current process, the supercapacitor heating has an exponentially decaying current curve. The total energy dissipated on the wire should be at least equal to the constant current heating.

In the charging stage, the voltage on the capacitor V increases exponentially and can be expressed with the input voltage U_0, capacitor capacitance C, battery inner resistance R and time t.

$$\frac{V}{U_0} = 1 - e^{-\frac{1}{CR}t} \tag{3.5}$$

At t = CR, capacitor charges to about 50%, we prefer this value to be in the magnitude of minutes. Since R=100-200 Ohm for lithium battery, if we expect CR = 200s, then we could set the capacitance value as

$$C = 1\,F. \tag{3.6}$$

At discharging stage, the voltage on the capacitor follows the exponential decay law

$$V = V_0 \cdot e^{-\frac{1}{CR}t} \tag{3.7}$$

where V_0 is the initial voltage, C is the capacitance, R is the wire resistance.

With C = 1F, R = 0.55 Ohm (two wires in parallel, 1.1 Ohm for each), the capacitor discharges 50% energy at t = 2s. We want to tune the initial voltage so that, at the half energy stage, the current through the SMA wire is still beyond the 4-amp requirement. As a result, the initial voltage should be at least around 10V. However, considering that it cannot transfer 100% energy to the capacitor, it has to be significantly higher than 10V to charge the capacitor within a reasonable time frame.

When the voltage drops to a certain value, the energy dissipated on the wire will be immediately transferred to the ambience instead of raising wire temperature, which we discuss in the thermal modeling in Chapter 4.

The exact value for battery voltage is decided by charge/discharge modeling. We still start the modeling with a trial of 25V on battery because this is a general voltage that we can achieve by assembling several off-the-shelf battery in series. The capacitance and voltage ratings depend on the charge time, discharge time, and energy storage requirement. We simulate these processes

here.
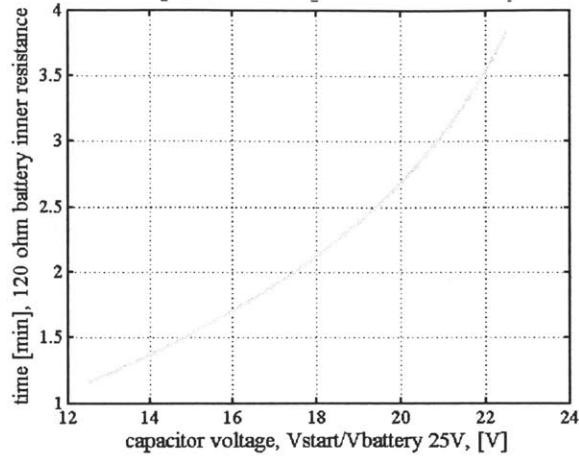
Figure 3-8: Charge time vs charge ratio with 25V battery

As shown in Figure 3-8, it takes up to 2 minutes to charge the supercapacitor to 18V, assuming we choose the voltage divider carefully enough so that the leakage rate is negligible for our purpose.
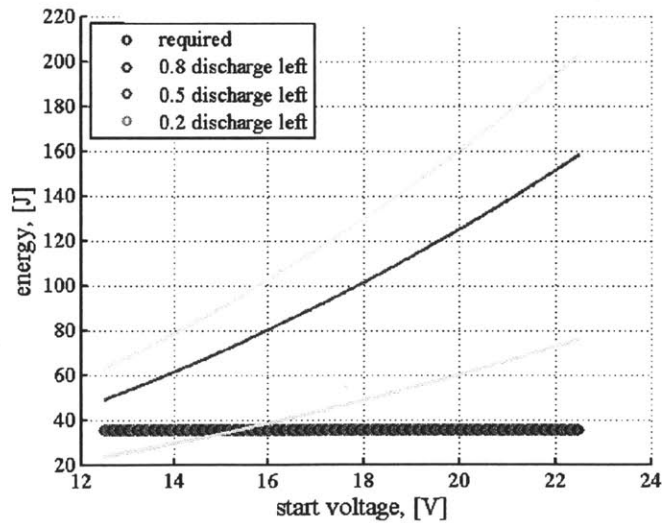
Figure 3-9: Energy comparison at discharge stage

In Figure 3-9, the dark blue line represents the total energy dissipation required on the wire to fully contract 5% in length. The other curves represent the dissipated energy from a certain initial voltage when the discharge stops at a certain level of charge left in the capacitor. The discharge

51

below 50% level turns out to be very slow and would be dissipated quickly into the ambience. As a result, we only count the energy above 50%, which we call functional energy. In short, the functional energy has to surpass the required constant current energy to make the whole system functional. At the same time, we want to minimize the initial start voltage both to reduce the charge time and to maximize safety protection for the embedded circuit.

According to our simulation, 14V turns out to be a reasonable value for our purpose with a safety factor of 1.5. This voltage largely depends on the specific application and operational requirement of the valve, and is a function of charge time, discharge time, and the actuation system dimensions. Future manufacturers can tune this value accordingly. However, in this thesis, we will use 14V as a reasonable example for the discharge initial voltage.
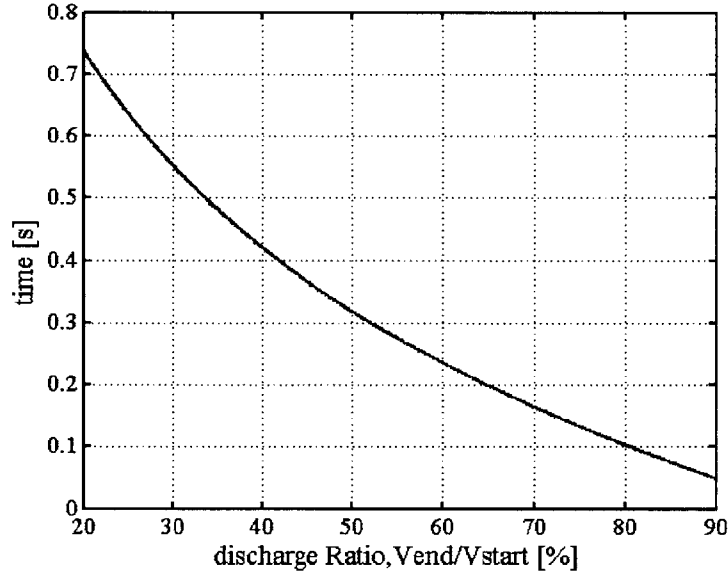
Figure 3-10:   Discharge time

Based on our analyses, we decide a capacitor with 1F capacitance and a 15V voltage rating is appropriate for our purpose.

Control capacitor

In the passive version of the control circuit, there is a small control capacitor at the sensor input side. In a real backflow event, the oil flow might not be continuous, i.e., it might alternate

between high conductivity oil and low conductivity gas, due to the erratic environment during valve failure. As a result, the signal might turn out to be below the MOSFET threshold for a period of time after the backflow is detected, and the charging process will pause. In order to solve this problem and maintain continuous charging, a small capacitor is installed in parallel with the sensor signal. Once there is a signal input from the sensor, it charges the capacitor first. When the capacitor is full, the charging process will be sustained by the capacitor regardless of the voltage from the sensor. Since there is only negligible current through MOSFET once it is turned on, this capacitor can technically keep it on for a fairly long time.

The total charge on the capacitor when fully charged at 5V is

$$Q = CU = 5C \qquad (3.8)$$

where C is the capacitance. The capacitor keeps draining due to the leakage current through the MOSFET.The total time it could hold the MOSFET on depends on the leakage current (10 uA for a typical general use MOSFET). As a result, the effective time is

$$T = \frac{Q}{A} = \frac{5C}{10\,uA} \qquad (3.9)$$

and it's a function of the capacitor capacitance C.

The whole charging process takes up to 3 minutes. With a large safety factor, a 1mF capacitor could keep the MOSFET on for 10 minutes. On the other hand, we want to keep this capacitor as small as possible to keep the charge time from the sensor to a minimum so as to improve response time.

Resistor

The control resistor in the voltage divider need to meet two goals. One is to keep it high enough so that the leakage current is low when the capacitor voltage is constantly driving a small current through the resistor. If this current is too large, the capacitor might never reach the required voltage.

Capacitor equilibrium voltage, V, is the maximum voltage the capacitor can reach with voltage divider resistance. At equilibrium, the leakage current through the monitor resistors $R_1 + R_2$ should be equal to the charge current from the battery.

$$\frac{Vo-V}{R} = \frac{V}{R1+R2} \qquad (3.10)$$

53

V_o is the battery voltage, and R is the battery inner resistance.

We have to keep this value as close as possible to the battery voltage of 25V.
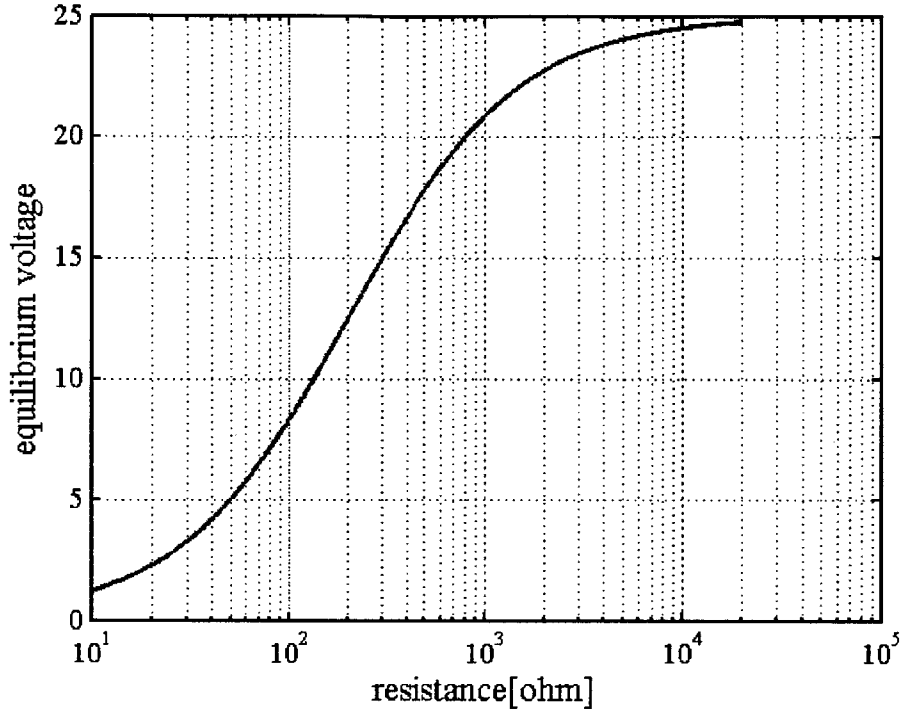
Figure 3-11: Equilibrium voltage with different voltage divider $R_1 + R_2$

As indicated by Figure 3-13, the sum of the voltage divider resistance has to be at least 10 kOhm to make the equilibrium voltage on capacitor reach the battery voltage.

The second goal is to adjust R1, R2 ratio meticulously to set $V = Vo \cdot \frac{R1}{R1+R2}$ equal to the threshold voltage of the MOSFET, where Vo is the target discharge voltage from the capacitor.

MOSFET

The metal-oxide-semiconductor field–effect transistor (MOSFET) is a transistor used for amplifying or switching electronic signals. Although the MOSFET is a four-terminal device with source (S), gate (G), drain (D), and body (B) terminals, the body of a MOSFET often is connected

54
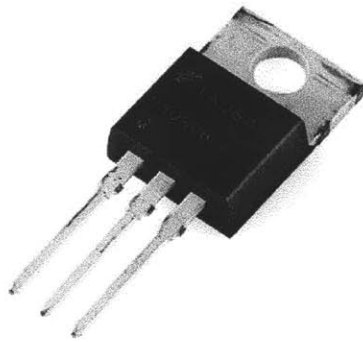
Figure 3-12: General use MOSFET, Digikey.com

to the source terminal, making it a three-terminal device. By far, the MOSFET is the most common transistor in both digital and analog circuits. Normally, the resistance between drain and source is extremely high, on the order of hundreds of Kohm, and it functionally forms an open circuit. When the input voltage on the gate terminal increases slowly, the resistance between source and drain will decrease nonlinearly up the point of a certain gate activation voltage, at which point the S-D resistance drops to near zero and actually forms a closed circuit. In this way, a MOSFET can be used as a switch in the circuit by changing the input voltage at the gate.

The voltage rating should be at least higher than the charge battery, 25V in our case. Work current ranges from 4A to 10A at peak with our design. Also, we would like to keep the gate voltage relatively low and the same for all the MOSFET and relay parts so that they can be output from the same battery.

Relay

A relay is an electrically operated switch. Many relays use an electromagnet to operate a switching mechanism mechanically. Relays are used where it is necessary to control a circuit by a low-power signal. A simple electromagnetic relay consists of a coil of wire wrapped around a soft iron core, an iron yoke that provides a low reluctance path for magnetic flux, a movable iron armature, and one or more sets of contacts. The armature is held in place by a spring so that when the relay is de-energized, there is an air gap in the magnetic circuit. When an electric current is passed through the coil, it generates a magnetic field that activates the armature, and the consequent movement of the movable contacts either makes or breaks a connection with a fixed contact, and closes or opens the circuit. When the current to the coil is switched off, the armature

is returned by a force, approximately half as strong as the magnetic force, to its relaxed position. Usually, this force is provided by a spring.

The purpose of having a relay control at the final discharge phase is to keep the binary logic. A typical MOSFET has a small drain-to-source current before it hits the threshold voltage. In contrast, a relay relies on a mechanical mechanism to turn it on and off. As a result, it is either on or off, with no grey zone in between. We do not want any current leakage through the wire as the capacitor is charged up. Otherwise, the wire will waste a considerable amount of energy at best, or, in the worst case, never reach the threshold voltage due to the constant leakage from the capacitor.

The turn-on/off voltages also come into consideration. We prefer that there be a huge difference between them. Once the relay is turned on at the turn-on voltage, the supercapacitor starts the discharge phase and the gate voltage on the MOSFET decreases accordingly. At a certain point, the control voltage on the relay will drop to the turn-off voltage (when the relay is turned off) and the discharging is over. If turn-on/off voltages are close, the relay will be turned off soon after it is on—before enough energy is dumped out of the supercapacitor and into the SMA wire.
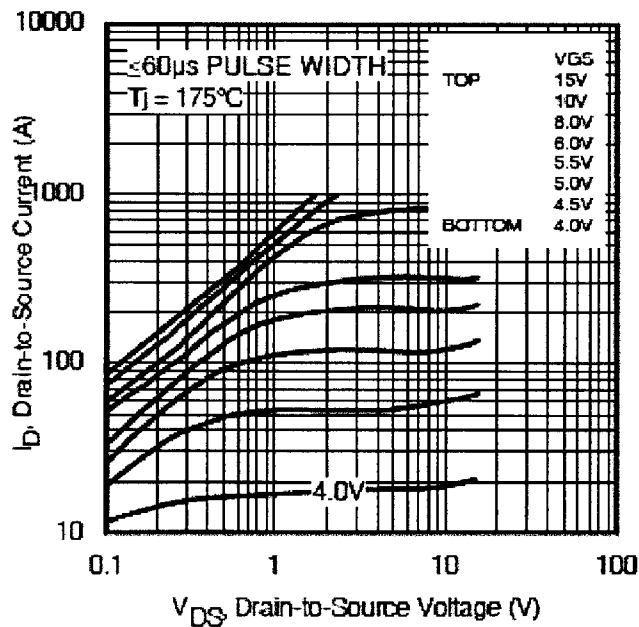
Figure 3-13: Electronic feature of MOSFET irf1324, Digikey.com

Table 3-1: List of parts for our prototype circuit.

Part type	Part# on Digikey.com [16]	Key features
Supercapacitor	283-3124-ND	C = 5F Vrate = 2.5V
Capacitor	P5514-ND	C = 1mF Vrate = 10V
Relay	PB1228-ND	Von = 3.75V Voff = 0.5V
MOSFET/BJT transistor	IRF1324pbf/ 497-2616-5-ND	Gate V = 4.1V
Battery	P666-ND	V = 3V E = 225mAh

3.1.2 PCB prototype

In order to test the reliability and functionality of the breadboard prototype, we manufactured a PCB version of the control circuit. A printed circuit board, or PCB, is used to mechanically support and electrically connect electronic components using conductive pathways, tracks, or signal traces etched from copper sheets laminated onto a non-conductive substrate. A PVC-based wiring board is manufactured according to computer-aided wiring design software before soldering the functional parts such as relays, resistors, processors, MOSFET, etc. It is cheap and fast to make and easy to implement for circuit prototypes.
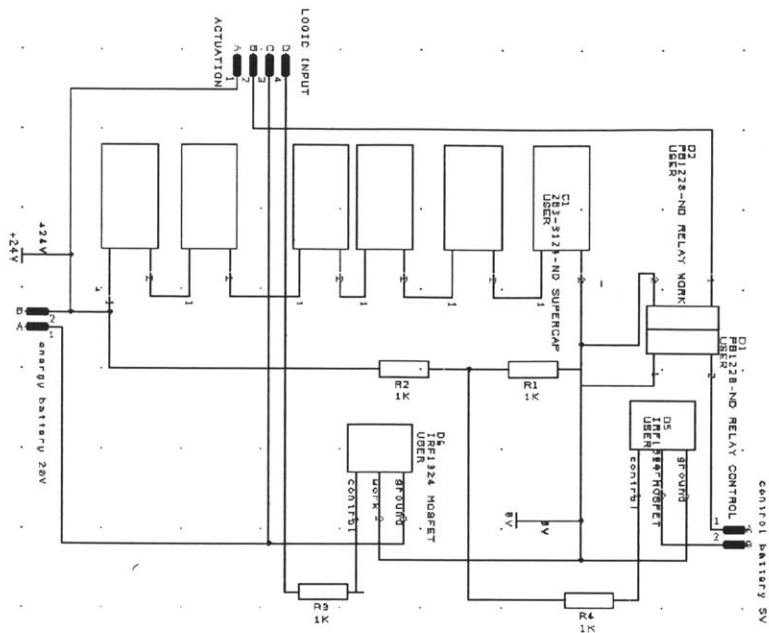
Figure 3-14: PCB schematics file, 4pcb.com
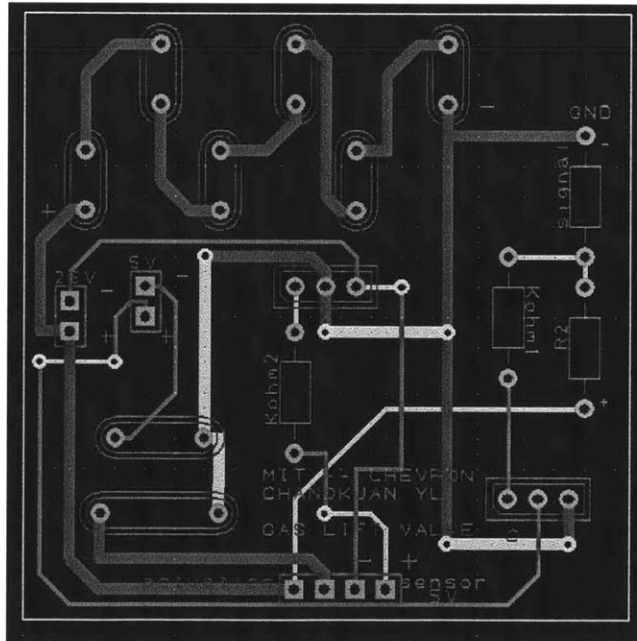
Figure 3-15: PCB layout file, 4pcb.com

On the PCB board, the copper wire connecting the supercapacitors and the output pins have to be extra wide to avoid electric burning due to the large current. The specific width depends on

the particular depth and the material from each manufacturer.
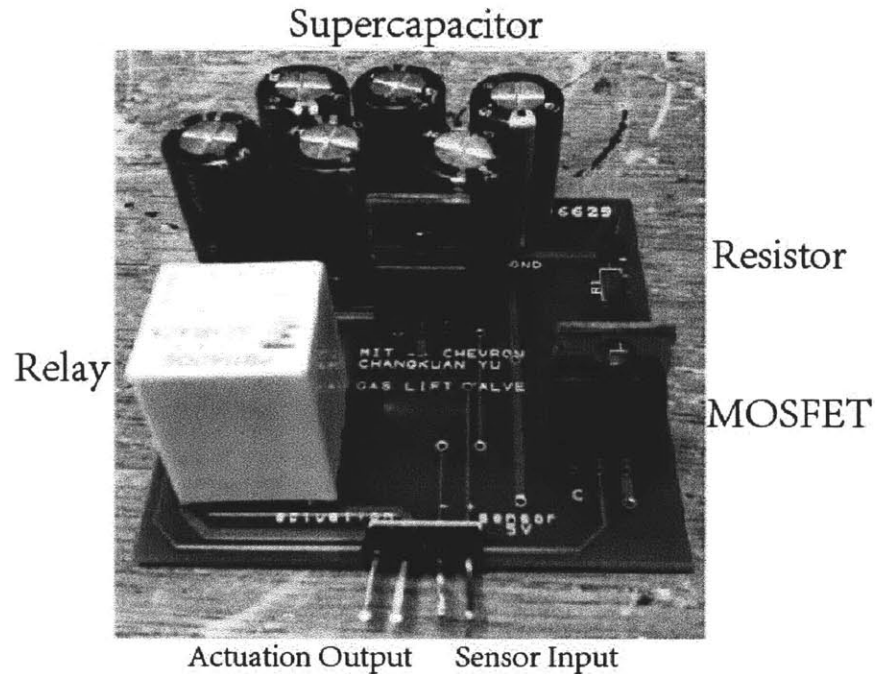
Figure 3-16: PCB prototype assembly, advanced circuit

3.2 Mechanical Integration

Integrating electronics into a gas lift valve may be a brand new idea to this industry. Due to the high pressure, high temperature, and corrosion, keeping the components alive is a major challenge for any design concept. We talk about the reliability and survivability of the electronics in following chapters and focus on the mechanical design here.

The current gas lift valves are designed for a particular mandrel of a certain length. There are over 3000 gas lift wells in the Gulf region alone [17]. Adding an electronics safety mechanism while keeping the current total valve length is desirable because replacing all the tubing and mandrels would require a huge investment and be a very slow process. Based on this assumption, we have to keep the gas lift valve external dimensions (i.e. length, diameter, inner gas orifice) the same, and we have to find extra space inside the valve body.
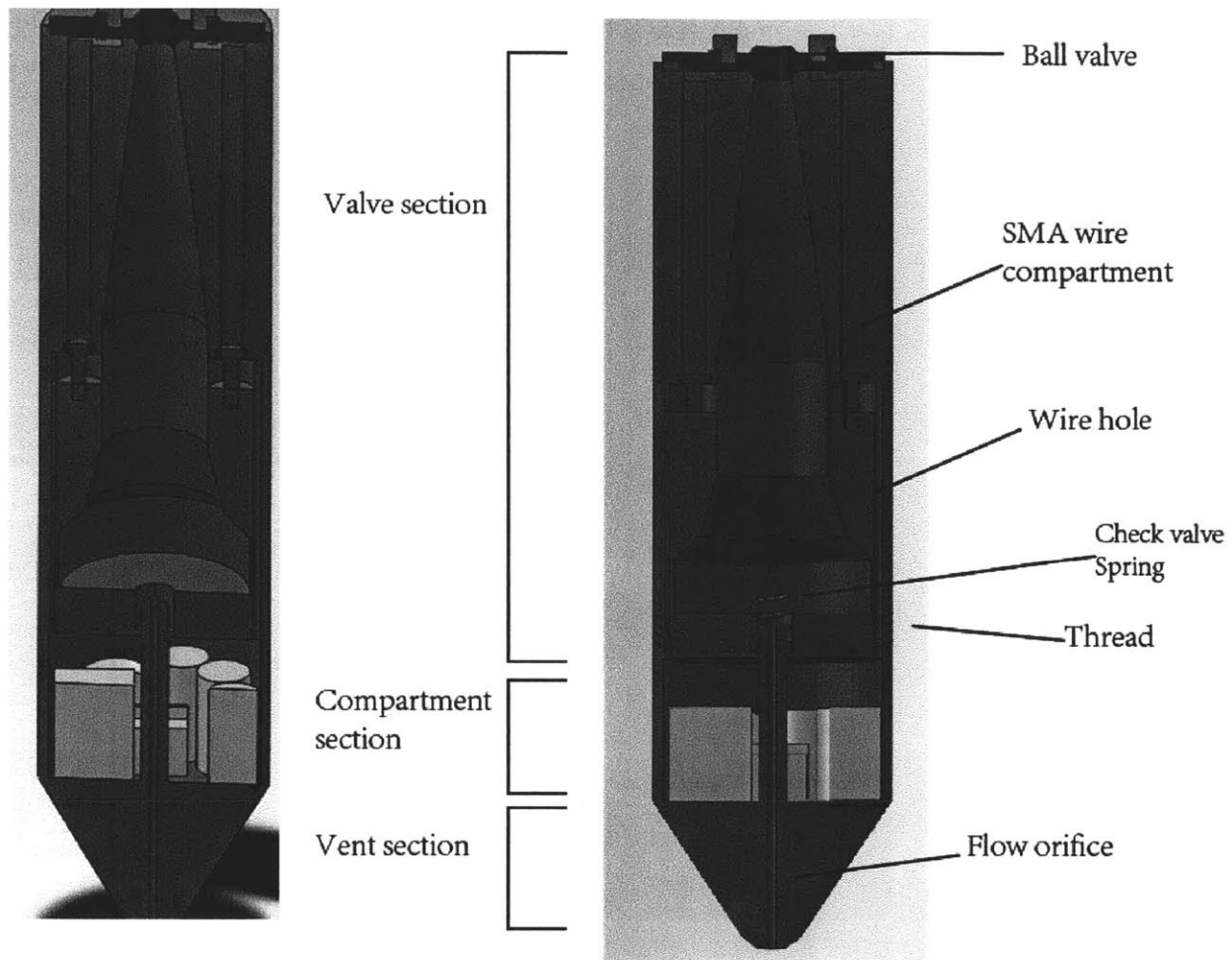
Figure 3-17: Valve annulus chamber design (VAC)

In this design, the annulus chamber takes up the originally solid part of the lower bottom vent section (see Figure 3-17) without changing the valve gas orifice. The top valve section and the bottom section (vent section and compartment section) are threaded together after installing the electronics. Electric wires go through the wire holes from the VAC to the shape memory alloy. Sealing and anti-corrosion coating are necessary at the thread. Also, in the VAC, the electronics have to be wrapped in anti-shock material because the valve is under up to 1000g of mechanical shock [17] during wireline installation. Electronics with a high shock rating might be another choice. The high rating electronics currently used in missiles have shock ratings up to 15500g

[18].

The VAC in current valve body has an upper limit volume of 1 in^3 as a structural strength requirement. With the off-the-shelf parts we have in the prototype, the total circuit volume is at least 3 in^3, on the same order of the magnitude as the requirement but still some distance away. The volume distribution is listed in Table 3-2. The major volume goes to the relay, over 50% of which is the housing package. Similarly, we bundled seven 3V lithium batteries to reach the required voltage, but we do not need that amount of energy.

The whole circuit system has to be custom made to be downsized and fit into the VAC.
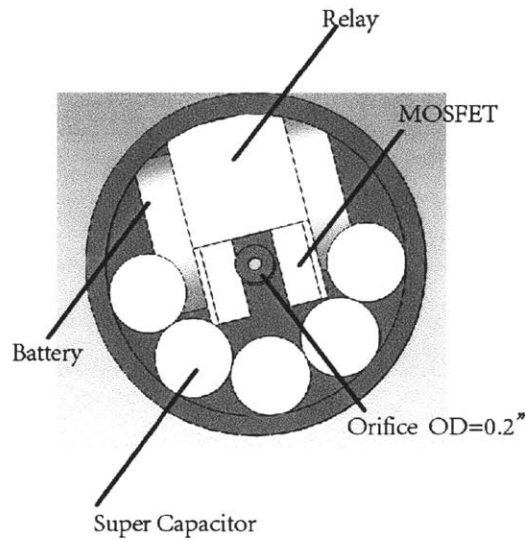
Figure 3-18: Cross section view of VAC

Table 3-2: Volume distribution in the part

Part	Volume (cubic inch)
Super capacitor	0.75
Battery	1 (off the shelf)
	0.01 (custom made, same voltage, less energy)
Relay+ accessories	1.25

3.3 Chapter summary

we presented the design details of the control circuit for the electronically-actuated safety valve and explained the criteria to choose the parts for the system. In addition, the way to integrate the circuit mechanically to the original valve is described in detail.

Chapter 4
SMA System Modeling

Xiang-Ming He [5] has researched Dynalloy shape memory alloy (SMA) thermal and heat transfer characteristics. This is the same wire we are testing in our prototype. We modeled the shape memory alloy based on his results and tried to predict the contraction behavior in both water and air, the ambient fluid during normal production and the unloading process. This work also lays the theoretical groundwork for testing the prototype system in a controlled-temperature water tank.

In addition, we modeled the wire strain-stress with different initial tensions to make sure we do not cause permanent strain by applying too much preloading for raising the transition temperature.

4.1 Heat transfer

We model the SMA wire heat transfer as a vertical cylinder dominated by natural convection. With different inclinations, the Nusselt number and heat transfer rate are highly dependent on the Rayleigh number. In fluid mechanics, the Rayleigh number for a fluid is a dimensionless number associated with buoyancy driven flow (also known as convection or natural convection). When the Rayleigh number is below the critical value for that fluid, heat transfer is primarily in the form of conduction; otherwise, it takes the form of convection. It may also be viewed as the ratio of buoyancy and viscosity forces times the ratio of momentum and thermal diffusivities.

Rayleigh number is calculated with the following equation and definitions:

$$R_a = \frac{g\beta}{\gamma\alpha} \cdot (T_s\text{-}T_\infty) \cdot x^3 \quad [19] \qquad (4.1)$$

$[R_a]$ Rayleigh number

$[g]$ acceleration due to gravity

$[\beta]$ thermal expansion coefficient

$[\gamma]$ kinematic viscosity

$[\alpha]$ thermal diffusivity$[x]$ characteristic length (wire diameter in our case)

We plug in the data for water and air: the Rayleigh values are 94.68 and 0.76 respectively, assuming $T_s = 100°C$ and $T_\infty = 25°C$. These values vary slightly with different T_s but are all on the same order of magnitude. With an effective Rayleigh number, we can find the corresponding Nusselt number on the experiment result from He's result and convert it to the heat transfer rate h value. Nusselt number is the ratio of convective to conductive heat transfer accross the broundary and can be calculated by the following equation and definitions:

$$Nu = \frac{hD}{K} \qquad (4.2)$$

[Nu] Nusselt number

[h] heat transfer rate

[D] wire diameter (0.02" for our case)

[K] conduction heat transfer rate of fluid

According to He's [5] experimental result, with an inclination angle of 1.5 radians (vertical), we plug in the corresponding Rayleigh number and obtain the Nusselt number for each case. Finally, we calculate the heat transfer rate for each case. The Nusselt number is the ratio of convective to conductive heat transfer across the boundary.
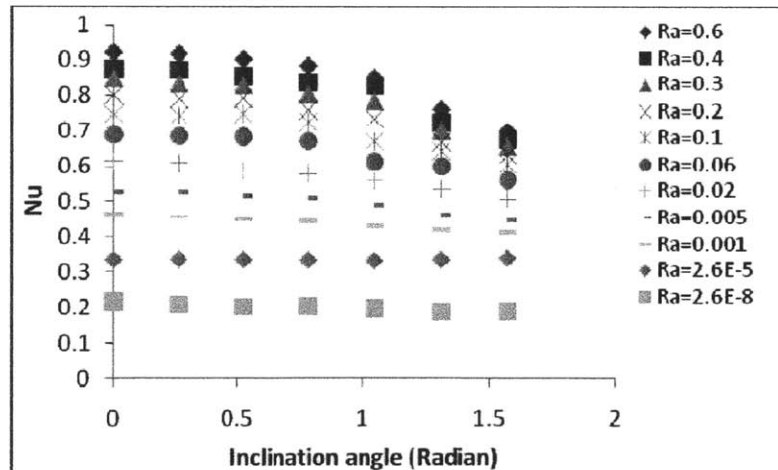
Figure 4-1: Nusselt number vs. (inclination and Rayleigh number) [5]

Finally, we obtain the heat transfer rate h in two materials:

$$h = 40 \quad W/m^2 \quad air$$

$$h = 600 \quad W/m^2 \quad water$$

These h values are the experimental heat transfer rates for SMA wire in water and air respectively.
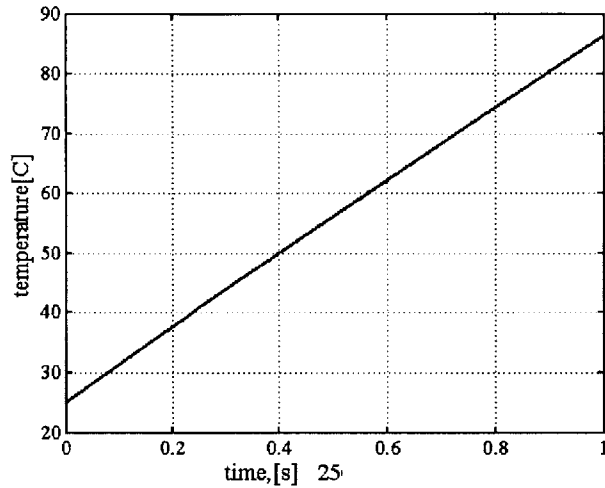
Figure 4-2: Heat transfer with constant current 4A in 25C air

We apply this model result to the wire with a constant heating current of 4A. The temperature rise curve is shown in Figure 4-2. The temperature will reach $T_s = 80°C$ contraction within 1s, which verifies the experimental data provided by Dynalloy [11]. This finding proves to a large extent that our heat transfer model is appropriate for this particular case.
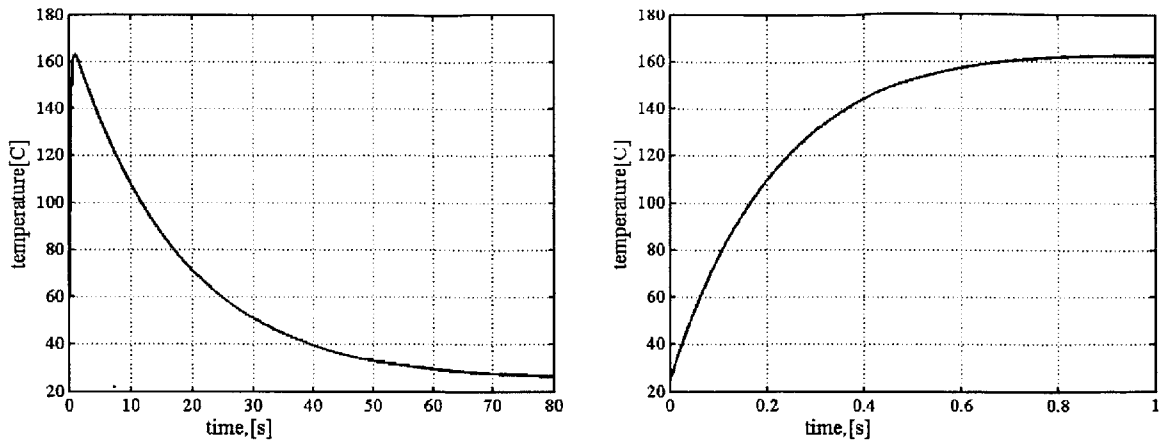
Figure 4-3: Heat transfer in 25C air with supercapacitor discharge,

right plot is the blow-up of the initial region of the left plot

Air environment simulation

Figure 4-3 simulates the heat transfer of wire in the air with 25°C ambient temperature in the lab with heating from supercapacitor current. Since the discharge is exponentially decaying during the process, the temperature is largely nonlinear. It takes up to 0.3s to drain the capacitor to a 50% level and, at that point, the temperature rises beyond contraction temperature, 80°C. As the current decreases, the temperature decreases from peak back to room temperature. In the real experiment, we can see the ball valve close immediately after the capacitor starts to discharge but reopen shortly after, due to the room temperature cooling.
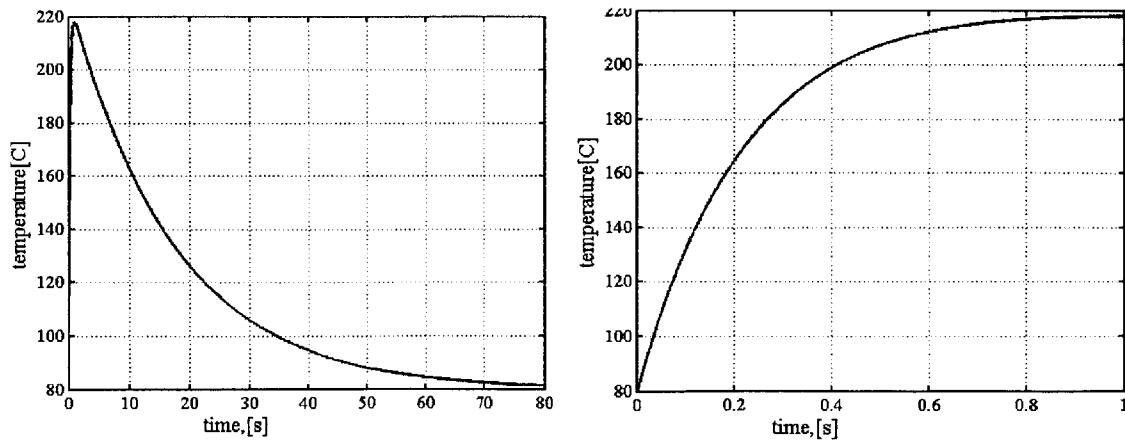
Figure 4-4: Heat transfer in 80C air with supercapacitor discharge

The typical temperature in the well is around 80°C, and it takes up to 90°C to complete the contraction for SMA wire. At around 0.3s, the wire temperature hits 180°C and cools back to ambient temperature. During this period, the shape memory alloy rapidly contracts and never expands back since its temperature is never cooled back below 60°C [11], where it would become martensitic from austenite phase.

The result from the air simulation indicates that it is infeasible for the SMA-based valve to close and stay closed in room temperature. We have to figure out a way to simulate the downhole temperature environment to test the functionality of the system.
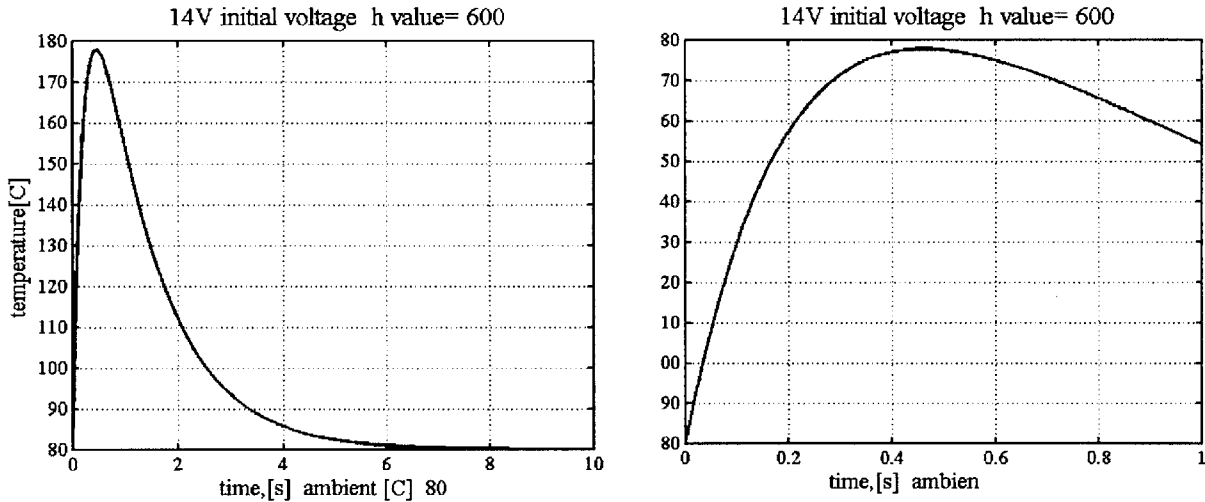
Figure 4-5: Heat transfer in 80C water with supercapacitor discharge

Water environment simulation

The wire heating process in water with 80°C ambience could still finish the contraction completely but take a little longer due to the fast heat transfer to the surrounding water. We also note that the maximum temperature it could reach decreases significantly. The crude oil heat conductivity is between air and water. Since the SMA wire will actuate perfectly in both air and

water, even during a real backflow with the worst case when the memory alloy compartment gets
filled with a mixture of air, natural gas, water, foam and crude oil, the system would still function
as expected.
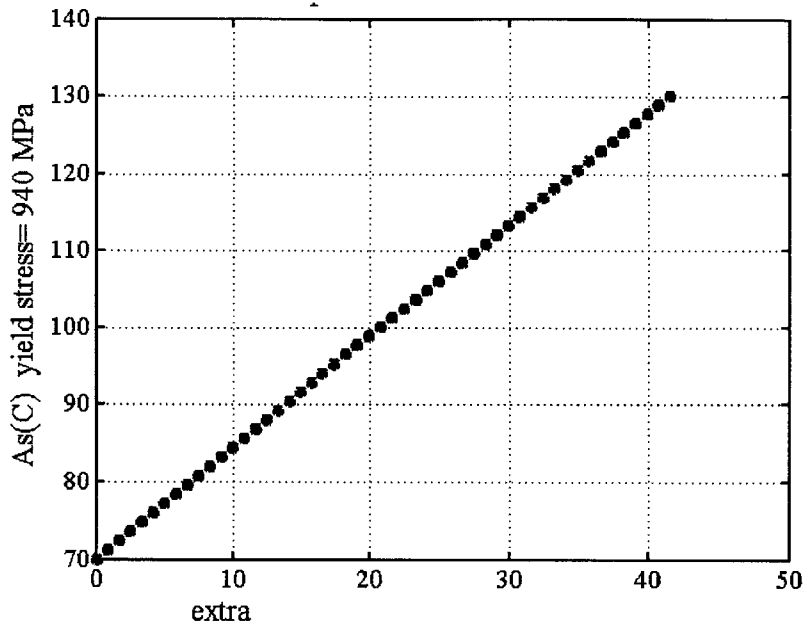
Figure 4-6: Increase in A_s due to additional initial tension from initial 172 Mpa

4.2 Structural strength

Too much initial tension on the wire could result in permanent strain and decrease the wire life
span. We want to make sure the initial tension we apply on the wire is well below the limit.

In our prototype, we use 0.02" diameter Dynalloy SMA wire. Each wire is 10 inches long. We
can change the transition temperature by applying different preloading on the SMA wires
according to $A_s = A_o + \frac{\sigma}{M}$. With a preloading of 172 Mpa [11], the initial transition temperature is
70°C. As we add extra stress on the wire, it increases up to 85°C with an extra tension of 10 Mpa.
However, this still far from the yield stress of 940 Mpa of SMA wire [5].

4.3 Chapter summary

we modeled the SMA wire with heat transfer to make sure the system could function well in case the compartment is filled with air, water, or a mixture of them with oil. Also, the structural strength model makes sure useful changes in transition temperature can be made by prestressing at a level that is no where near the yield stress.

Chapter 5

Sensor selection

The circuit system is based on the feedback signal from the sensor system. We measure the distinct features of crude oil that are not affected by pressure and temperature change. This sensor has to run at a very low power consumption, e.g. 1mW, and should be able to survive in high corrosion environment.

5.1 Crude oil characteristics

Crude oil is a naturally occurring flammable liquid consisting of a complex mixture of hydrocarbons of various molecular weights and other liquid organic compounds that are found in geologic formations beneath the earth surface. It is a highly conductive material. Although pure hydrocarbon has extremely low conductivity, the non-pure chemical from the reservoir, e.g. calcium minerals and/or ferric contaminants, increases the crude oil mixture's conductivity dramatically.

Crude Oil	Resistance (Ohm-cm)	
West Texas	3.0	
Arabian Light	1.5	
Arabian Heavy	1.1	
Alaskan North Slope	1.0	INCREASING
Maya	0.95	CONDUCTIVITY
BCF 17	0.9	
Lloydminster B	0.6	

Table 5-1: Resistance characteristics of crude oil from different regions [Weatherford]

In addition, fluid state crude oil is highly opaque and attenuates infrared and visible light to nearly zero intensity within millimeter scale distance. The aerated oil foam has a much higher transparency but still differs greatly from gas or liquid water.

5.2 Turbidity sensor

Turbidity is the cloudiness or haziness of a fluid caused by individual particles (suspended solids) that are generally invisible to the naked eye, similar to smoke in the air. Crude oil turbidity differs from that of water and gas due to the large amount of solids. There are multiple ways to measure and record turbidity but the SI unit system lacks a standard unit for it. In this thesis, we use a percentage-based unit. With any constant intensity through a constant-dimension fluid, we set the turbidity through perfectly clear air to 0%, where the light can come through with 100% intensity. We set the turbidity to 100% when the fluid can perfectly block the light. This unit may not be a general unit used to measure any dimension between the sensors, but it is sufficient for our controlled-dimension design. Due to the lack of online data on turbidity of different materials, we set up our own test equipment to measure it.

We use an infrared-based photoresistor emitter and receiver from LITE-ON Inc. [20]. A photoresistor or light dependent resistor (LDR) is a resistor whose resistance decreases with increasing incident light intensity; in other words, it exhibits photoconductivity. In our device, the emitter is constantly sending infrared light through the test sample with equal intensity. The test sample stays within a constant dimension container to ensure that the distance between the emitter and receiver stays the same from sample to sample, e.g. 0.5 inch in our case. The receiver photoresistor is connected in series with a 500 Ohm resistor and forms a voltage divider with 5V input. By measuring the voltage on the photoresistor, we can calculate its current instant resistance with the following equation and definitions.

$$R = R_r \cdot V / (V_{input} - V) \tag{5.1}$$

$[R]$ photoresistor instant resistance

$[V_{input}]$ supply voltage

$[V]$ receiver voltage

$[R_r]$ constant resistance in series
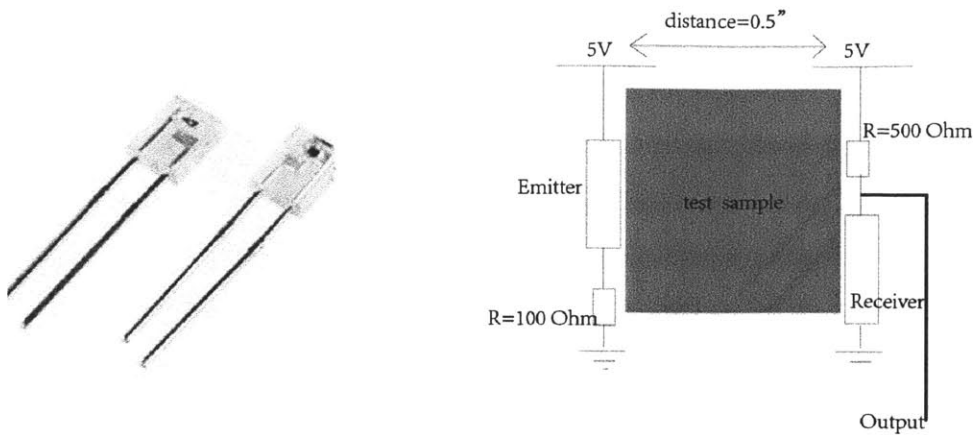
Figure 5-1:Photoresistor [20] and turbidity test equipment

The resistance increases dramatically from air to crude oil due to the attenuation of infrared light. In the gas lift production environment, the resistance increases by a factor of over 100 from normal production to backflow event as the orifice is filled with crude oil. This resistance data is sent to the microprocessor and then stored and analyzed to make decisions about whether to shut down or not.
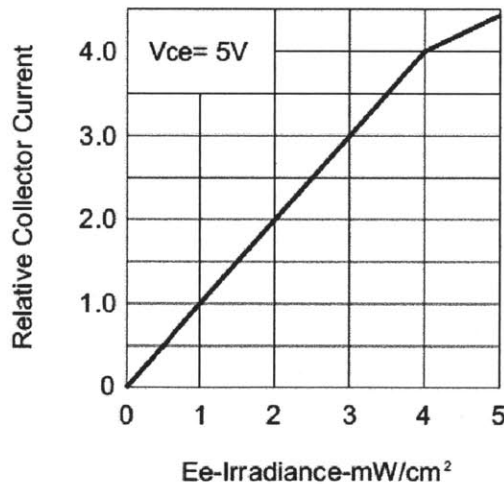
Figure 5-2: Photoresistor [20] current with light intensity under controlled voltage

Figure 5-2 shows that, within our operation region of infrared intensity, the current through the photoresistor is proportional to the light intensity shined on the sensor with a constant voltage. The current on the constant resistor is equal to the current through photoresistor and is much

easier to monitor than photoresistor current. We convert the resistance data to the percentage-based turbidity data. The current on the constant resistor follows Ohm's Law

$$\text{Current} \quad = \quad \frac{V}{resistance} \; , \tag{5.2}$$

where V is the voltage on that constant resistance.

This current is also proportional to the light intensity shined on the sensor.

$$\text{Current} \quad = \quad \text{constant A} \cdot \text{intensity} \tag{5.3}$$

With our customized unit , the intensity could be expressed as the original intensity with perfectly clear air multiplied by on minus the turbidity value in the test sample

$$\text{Current} \quad = \quad \text{constant A} \quad \cdot \quad \text{original intensity x (1-turbidity)} \tag{5.4}$$

After we plug 5.4 in 5.3 and combine it with 5.2, we have the relation between the voltage on the constant resistor and the turbidity value in the test sample

$$\frac{V}{1-turbidity} = \text{constant B} \tag{5.5}$$

$$= \text{resistance x constant A x original intensity}$$

$$= V \text{ (through air)}$$

Constant B is the constant product of constant resistance, constant A and the original intensity, and is equal to voltage data with clear air since the turbidity of air is set to be 0. With this equation, we can find the fluid turbidity given the voltage on the constant resistor in series.

Figure 5-3: Turbidity test with photoresistor resistance result

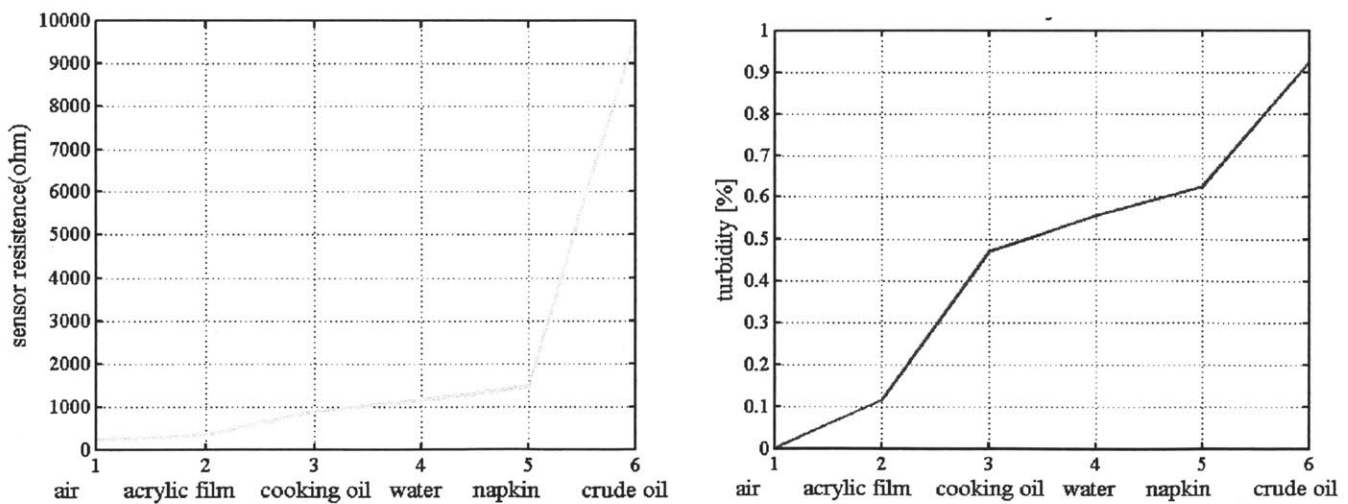We choose infrared sensors because infrared is less likely to be interfered with by the background light and easier to attenuate compared to shorter wavelength light. Although the downhole environment is completely dark, we still need to filter out the background light noise when we test, tune and reset the sensor on the ground before installing the valve.

Our current emitter from LITE-ON Inc. runs at 75 mW. For a more reliable system, it needs to run below 1 mW by sending out less infrared and turning on once every 24 hours for a few seconds to save energy.

A useful feature of the infrared emitter is the half sphere lens. It uniformly scatters the infrared rays in all directions. As a result, any point with the same absolute distance on the opposite side will receive an equal intensity light. This decreases the effort required to tune and zero the initial feedback before installation.

5.3 Conductivity sensor

Electrical resistivity quantifies how strongly a given material opposes the flow of electric current [22]. A low resistivity indicates a material that readily allows the movement of electric charge.

Electrical conductivity or specific conductance is the reciprocal quantity and measures a material's ability to conduct an electric current. It is commonly represented by σ. The SI unit is simens per meter (S/m). As shown in the Table 5-1, the conductivity of crude oil ranges from 30 to 170 S/m. In contrast, water conductivity is $5.5 \cdot 10^{-6}$ S/m for pure water and 5 S/m for sea water [23]. The increased conductivity is due to the increased minerals and solid material content. Air electrical conductivity is so low that we can consider it zero compared to water and oil.

A proper conductivity sensor for our purpose must be small, immune to corrosion, and able to measure conductivity from 0 to 200 S/m. Accuracy is not a major concern in our case because the sensor needs only to distinguish low conductivity, i.e. 0—2 S/m for water and gas, and high conductivity, i.e., over 150 S/m for crude oil.
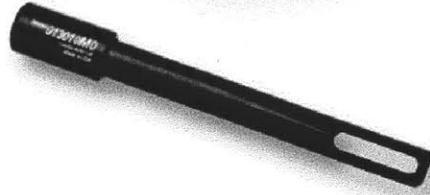
Figure 5-4: General use conductivity sensor probe [31]

One general-use large-range conductivity sensor from Thermo Scientific is Orion A222 with a test range between 0 and 300 S/m and superb sensitivity of 0.001 uS/m. The test probe is a pencil-size container with constant dimensions between two test electrodes. The sensor monitor passes a constant voltage through the electrodes. With a different conductivity in the test section, the output current varies linearly. A low current indicates a low conductivity.

The resistance of the test material follows the resistance rule:

$$R = \frac{\rho l}{A}$$ [R] resistance

[ρ] material resistivity

[L] distance between electrodes

[A] cross section area

In the test probe, the dimensions of test materials, i.e.length and cross section area, are controlled. By measuring the resistance, we can calculate the resistivity coefficient, and the conductivity coefficient is the reciprocal of that value. This conductivity signal is sent, stored and analyzed in the microprocessor to help make decisions regarding emergency shut down.

Both the outputs from these two types of sensors are analog. We have to implement proper filters to process the noisy signals to collect helpful results. Sensor signal processing is a mature technology and is beyond the scope of this thesis. However, it is a necessary procedure for the foam effect we will discuss later.

5.4 Temperature sensor

We can also detect a backflow event with a temperature sensor based on the temperature change rate. During normal production, the temperature drift of the whole valve and the reservoir can be as slow as $1°C$/month. However, during a backflow event, when the foam oil goes through the orifice, the temperature in the orifice changes as fast as several degrees per minute. We can

record the temperature every minute for latest time period, e.g. 1 hour, and calculate the temperature change rate. When the rate is above the predetermined threshold, which is above the physical upper bound of natural drift rate, we will start the actuation procedure and shut down the valve.

Figure 5-5 shows an example case we tested in the lab. The waterproof temperature probe is placed in a water container. Hot water and cold water are poured into the cup alternatively to simulate the temperature change in the valve orifice. In this example, we constrain the time frame to the magnitude of minutes and increase the temperature change rate to finish the test within a reasonable time. Temperature data is recorded at 4 Hz. The increase threshold is $0.2°C$ /s. Every time we obtain new temperature data point, we compare it with the data 5s earlier and check whether the difference is above the threshold rate multiplied by the time interval. Finally, as soon as the rate is beyond the threshold, we start the charge stage on the supercapacitor and discharge at predetermined voltage.
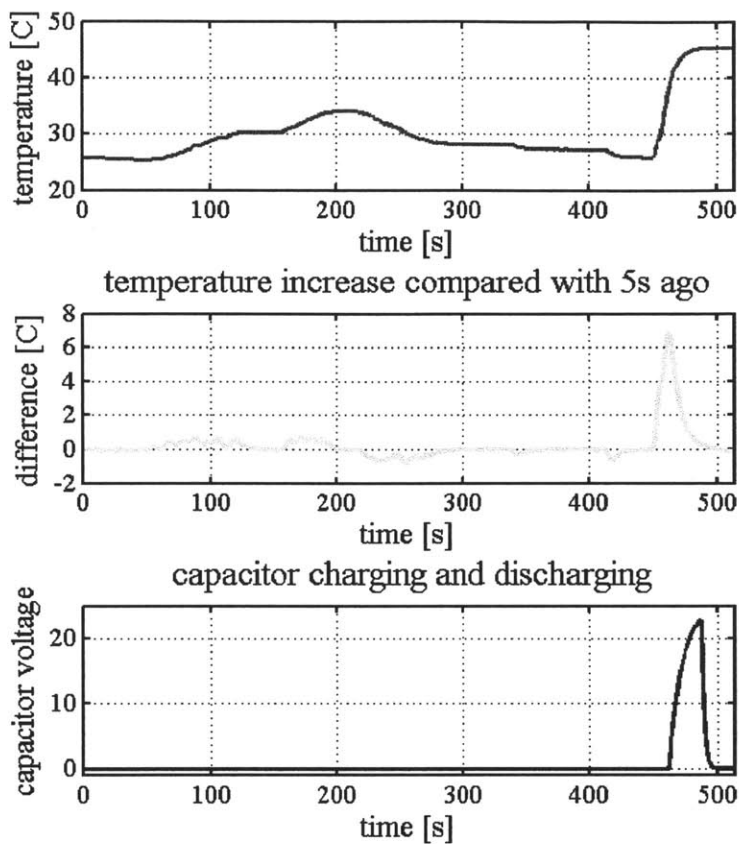
Figure 5-5: Temperature change rate and decisions

Since the thermocouple is shielded with a metal sheath, it has a physical filtering effect that can eliminate the high frequency noise due to the large heat inertia on the metal part. In the real valve, where the thermocouple could be in direct contact with oil, noise could be a serious issue in decision making. More logic could be implemented based on the sensor data. For example, the microprocessor records the temperature change rate for a long enough period. The system actuates only when the rate is above the threshold for the entire period. In addition, signal processing and noise filtering could be implemented on the microprocessor to make smarter decisions.

5.5 Foam effect

In the main tubing, due to the aerating process, the major material coming through is a foam-like crude oil filled with bubbles. As a result, the data collected from these sensors is constantly vibrating around the mean value. Depending on the amount of gas and bubbles, the value could vary drastically from the nitrogen gas level to the complete crude oil level.

If we design the valve to shut down after tracing the least amount of crude oil, we could set a very low threshold value for the decision mechanism, and keep track of the maximum value for each sensor. As soon as the maximum value surpasses the threshold, the system is actuated immediately.

A more sophisticated way to deal with the data is to filter out the high frequency data, keep the low frequency noise, and calculate a weighted average of the recent data. A decision based on this value would be more reliable and eliminate false alarms due to the sensor noise.

We also set up a test system to collect the turbidity sensor data with the foam effect. The turbidity sensors are placed at the opposite sides of a transparent container filled with water and cooking oil respectively. Air at constant flow rate is pumped to the bottom of the container. Therefore, bubbles form and float to the surface, blocking the passage of infrared light through the fluid. We monitor the photoresistor resistance and observe the attenuation of the infrared. A larger resistance indicates a more attenuated infrared light and a greater turbidity. It turns out that the bubbles will distort and block the light almost completely for oil due to the large difference in refractivity between oil and the air in the bubble. For this test, the photoresistor is in series with a 19 Kohm resistance with a 5V operating voltage.
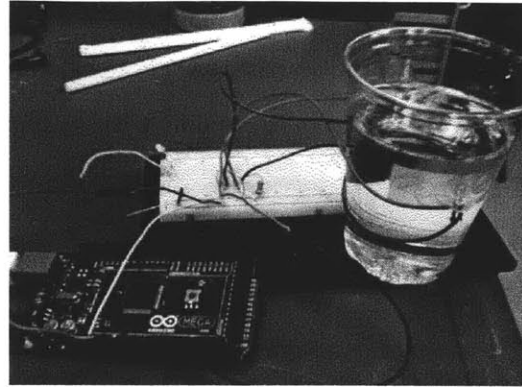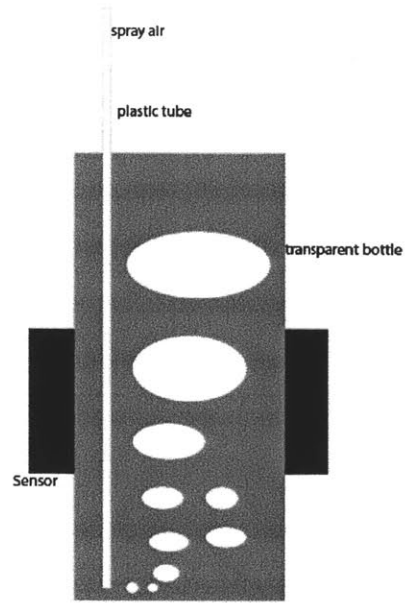
Figure 5-7: Turbidity test equipment
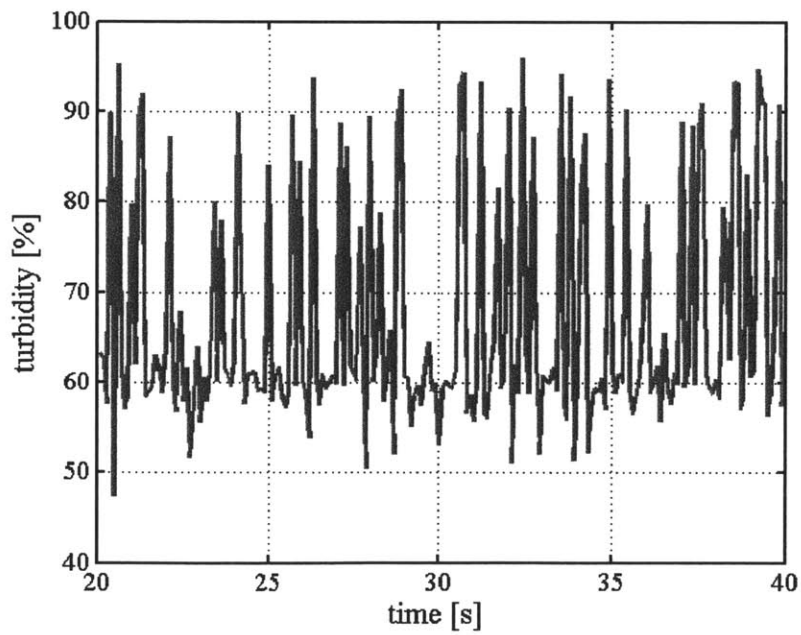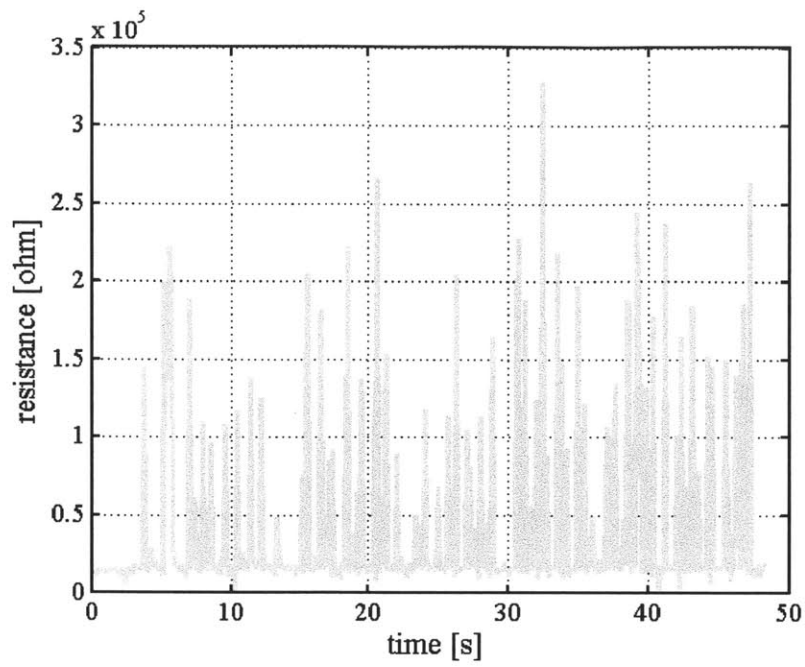
Figure 5-8: Water bubble test experiment result, pure water 60% turbidity

With relatively low viscosity for water, more small bubbles form and scatter the infrared more uniformly and continuously. The bubbles can refract the light to a large extent. As a result, no light is shined on the sensor. This attenuation mechanism is different the absorption and reflection mechanism of the pure material.
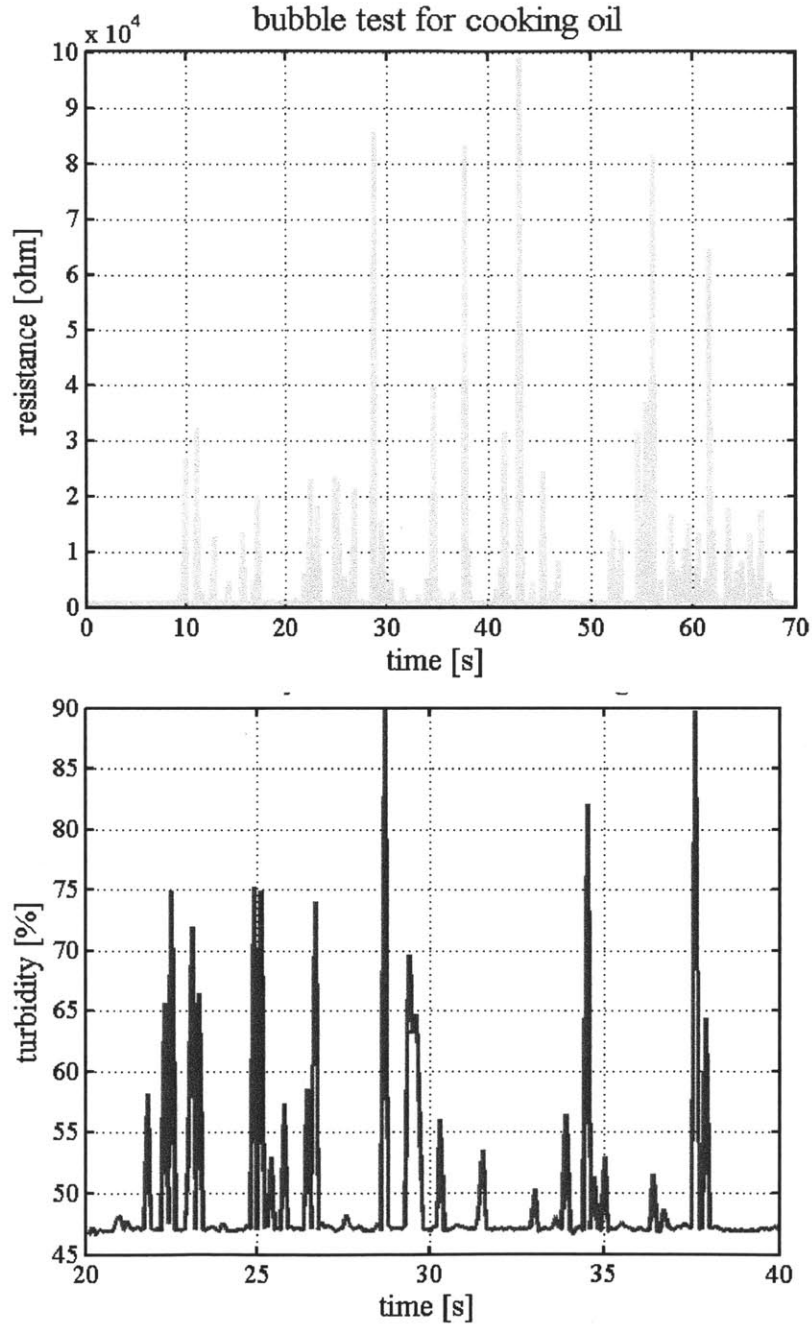
Figure 5-9: Oil bubble test experiment result, pure cooking oil 47% turbidity

The bubbles in the cooking oil with the same gas flow rate have a larger size due to the high viscosity. These large bubbles refract the light to a great extent. The bubble effect makes the threshold-based actuation logic much easier. Because the foam-like material with bubbles has much higher turbidity than pure material itself, if we set the threshold as the minimum signal from the pure material, the foam product could still lead to the correct decision of whether to shut down the valve. With this test, we are sure the turbidity sensor could distinguish air, pure fluid material and fluid with bubbles.

5.6 Chapter summary

we reviewed different sensors we can integrate in the control circuit and the signal characteristics of each one. At the same time, the foam effect on these sensors is investigated with experiment. The sensor can distinguish air from pure material, and foam material from the pure material.

Chapter 6

Survival Test

To function well in the harsh high pressure, high temperature, high corrosion environment, the electronic system has to survive under $80°C$ and up to 3000 psi. We ran tests to prove the system's reliability. Because we do not have access to a test facility that can simulate the downhole environment in terms of both high pressure and high temperature, we tested two levels—individual components and system PCB board—under pressure and temperature respectively. In this way, we could also decouple the effect from temperature and pressure on the electronic parts. The four major parts tested were the MOSFET, lithium battery, supercapacitor, and relay. We measured the major electrical features before putting them through the test and measured the same feature again after the test was complete.

6.1   Component test

For the pressure test, we have a pneumatic static press with pressure capacity up to 50000 psi. It pumps high pressure gas to increase the chamber pressure. All the components are wrapped in a plastic bag to prevent short circuiting due to the oil and stored in the pressure chamber for one hour under 5000 psi, 2000 psi more than the design target. During the test, the plastic bag is immersed in the hydraulic fluid. To additionally avoid short circuiting due to oil contaminants in future electrical tests, we may coat the parts with wax before the pressure test in oil.

For the temperature test, we use a vacuum oven. A different set of components is stored in a glass container in the oven to prevent direct contact between the electronics and the oven inner surface. In this way, the parts will be uniformly heated by the hot air inside. The heating lasts for 24 hours under $90°C$, $10°C$ more than the design target.
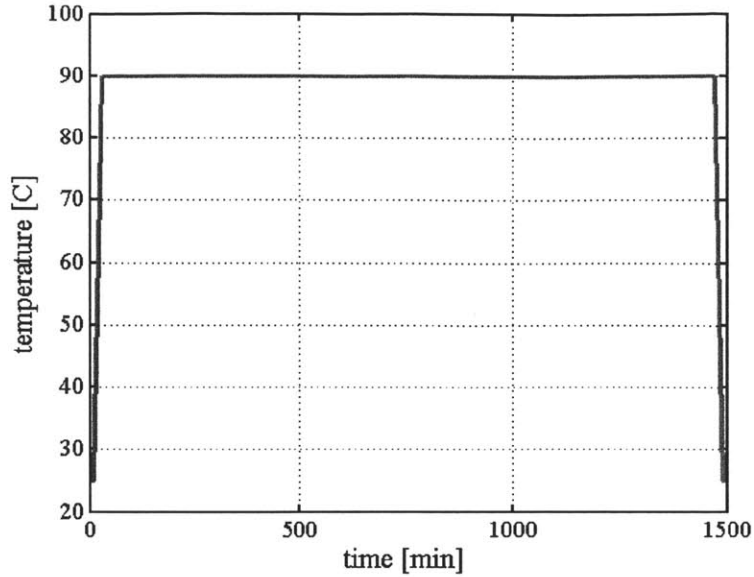
Figure 6-1: Temperature sequence in a vacuum oven

Component test result

Each test includes three sets of same parts, each of which is explained below:

A. Original parts

B. Pressure tested parts   5000psi, 1 hr

C. Temperature tested parts   90°C, 24 hr

Table 6-1: MOSFET test result

MOSFET IRF1324	Close circuit resistance /open circuit resistance(ohm)	Activation voltage (V)
A	0.1/286K	4.1
B	0.1/280K	4.1
C	0.1/290K	4.1

The MOSFET must have high enough open circuit resistance when turned off to keep the energy leakage rate low and save energy. Also, the closed circuit resistance should be low when turned on to ensure that the system can be actuated as expected. Activation voltage determines the initial voltage on the supercapacitor at actuation. It has to stay constant to ensure that the performance of shape memory alloy stays the same for each case.

With the electrical double-layer technology in the supercapacitors, there are numerous

nanometer scale bubbles inside, and they are strong enough to withstand such high pressure. In addition, since most of the material in the MOSFET is metal and silicon, it remains intact under high temperature. These tests demonstrate that the MOSFET could survive in the downhole environment of both high pressure and high temperature.

Table 6-2: Battery test result

6V Lithium Battery P143-ND	Voltage(V)	Inner resistance(Ohm)
A	5.69	26.3
B	5.56	24
C	5.88	56

The battery must keep enough energy and voltage to actuate the system and also have low enough inner resistance to keep a relatively high discharge rate. The maximum discharge rate is the ratio between the voltage and the inner resistance. All batteries constantly self-discharge, and most of them self-discharge faster under high temperatures. The battery shows a drop in energy in the form of a constant voltage with a high inner resistance. For a battery that runs out of power, the voltage stays the same but the inner resistance is too high to output any significant current. To measure the inner resistance, we connect the battery to a 10 Ohm resistor and multimeter in series and close the circuit. By reading the current on the multimeter, we can calculate the inner resistance, r, with the rule current = battery voltage/(R+10)

In an extreme temperature test, we put the battery in an oven at up to 150°C, which caused an immediate fire and explosion. The lithium ion battery technology turns out to be unreliable under high temperature. These test demonstrate that the battery could function under high pressure but has significantly higher inner resistance under high temperatures.

Table 6-3: Relay test result

RELAY	No damage to the copper coil
PB 766-ND	Activation/Release voltage unchanged

The only feature of concern for the relays is the activation voltage. This value stays the same for all three cases. Most of the parts inside are metal mechanical, such as the armature, coils, and frame, with no enclosed bubbles. As a result, they can survive both high pressure and high temperature.

Table 6-4: Capacitor test result

5F/5V super capacitor 283-3520-ND	Capacitance (F)
A	3.5F
B	4.1F
C	4.4F

The only feature of concern for the supercapacitor is the capacitance. Since it has no inner resistance besides a negligibly small parasitic resistance, the output current is always unlimited. We charge the test sample from 0V with a constant 2V voltage source. The capacitor is connected in series with a 10 Ohm resistor to restrict the current and slow down the charging stage.

The voltage increase follows an exponential curve $V = V_o(1 - e^{-1/(CR)*T})$. We count the time in seconds from 0V to 1.73V, when the time should be equal to 2RC, where R is the resistance in series and C is the capacitance value. Through simple calculation, we can determine the capacitance on the supercapacitor. This test demonstrates that the capacitance change is within tolerance.

6.2 Chapter summary

we documented the high pressure/high temperature test for each part in the control circuit and proved they could survive and function well in the downhole harsh environment.

Chapter 7

System Functionality Test

We have proven that the three major subsystems—SMA actuation, sensor, and energy—could function and survive in the downhole environment. We need to prove that the whole system could function well. To this end, we designed a system functionality test in which we simulated the production environment in the lab, pumped water through the prototype orifice, collected data from the sensor, made proper decisions with the microprocessor, and shut down the production valve within the design time frame. In this test, although it's not with the true scale and at the true pressure, all the other key aspects are accurate.

7.1 Test Facility

The SMA will cool down to ambient temperature and almost immediately expand in room temperature. We have to set up a controlled environment with a temperature below As to avoid actuation due to ambience and above Ms to avoid expansion when the wire cools down to ambient temperature. Also, we want to keep this temperature as low as possible to make the system safe and easy to handle. According to the data sheet from Dynalloy [11] wire, $60°C$ is the lowest possible temperature for this purpose.

We built a $60°C$ water tank for our test. We choose water rather than oil because its large specific heat could provide a large heat inertia and the system is more stable. Also, fluid water has high heat transfer rate compared with gas. As a result, the temperature within the tank would be relatively uniform.

The control algorithm is based on a digital temperature sensor and two heat exchangers. Each exchanger is plugged into the grid through a general-use relay controlled by the microprocessor. The temperature data is constantly sent to the processor. When the tank temperature is below $55°C$, both heat exchangers are turned on. Between $55°C$ and $60°C$, only one exchanger is turned on. Above the target $60°C$, both exchangers are off, and the system is cooled down by natural convection above the water surface and direct conduction between the tank bottom and the bench.

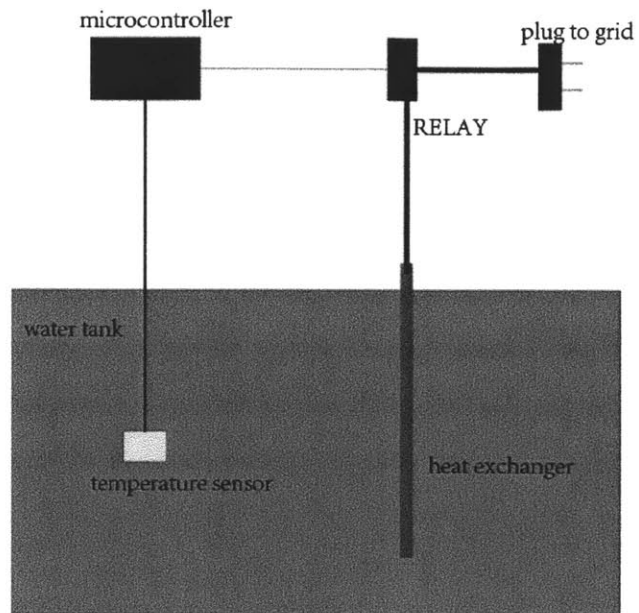The hardware set-up is shown in Figure 7-1.

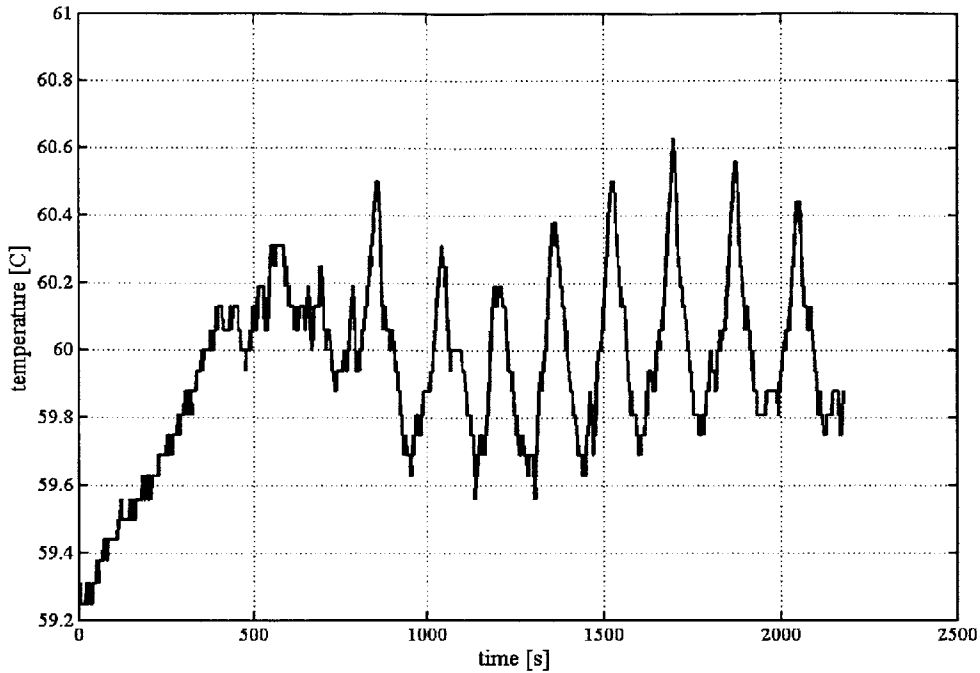Figure 7-1: Constant temperature water tank design and hardware

Figure 7-2: Water temperature fluctuation

The system functions well with a $0.6°C$ max error, as shown in Figure 7-2. One way to attenuate the error is to implement pulse-width modulation (PWM) control on the heat exchangers. PWM is a modulation technique that conforms the width of the pulse based on a modulator signal information. Although this modulation technique can be used to encode information for transmission, its main use is to allow control of the power supplied to electrical devices. The average value of voltage fed to the load is controlled by turning the switch between supply and load on and off at a fast pace. The longer the switch is on compared to the off periods, the higher the power supplied to the load. The equivalent power supply is equal to the average value over the whole period, the duty ratio, which describes the proportion of "on" time to the regular interval or "period" of time.

In our device, the major reason for the $0.6°C$ temperature overshoot is the heating from heat exchanger after it is turned off. The exchanger has a large heat inertia and will stay hotter than the water for a fairly long time after it is turned off at $60°C$. As a result, the water temperature keeps heating up, which causes a considerable overshoot. With the PWM control method, between $55°C$ and $60°C$, we can turn on the heat exchanger for 0.3s every 1s to decrease the heating power and effectively minimize the overshoot. This technique is

89

implemented by sending a HIGH/LOW signal alternatively from the microprocessor to the heat exchanger relays . Figure7-3 shows a typical signal example for PWM control.
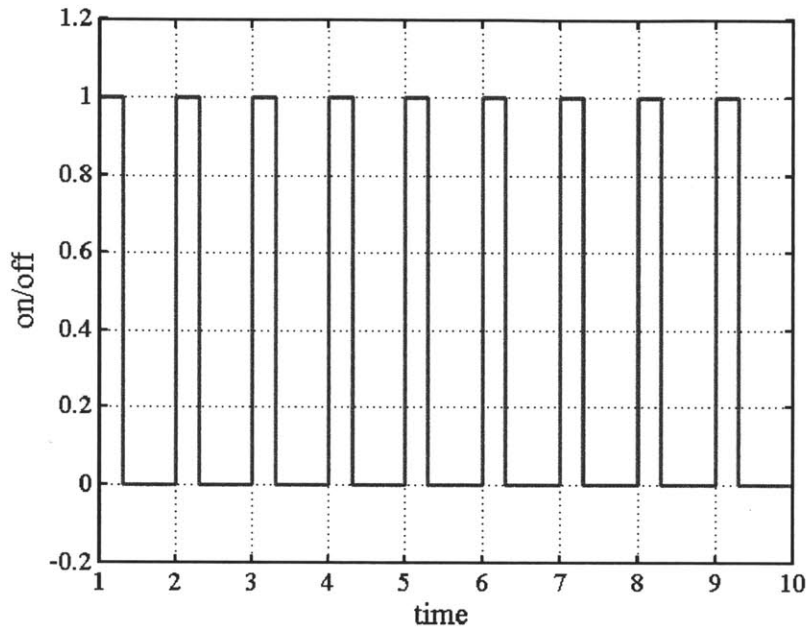

Figure 7-3: PWM control signal
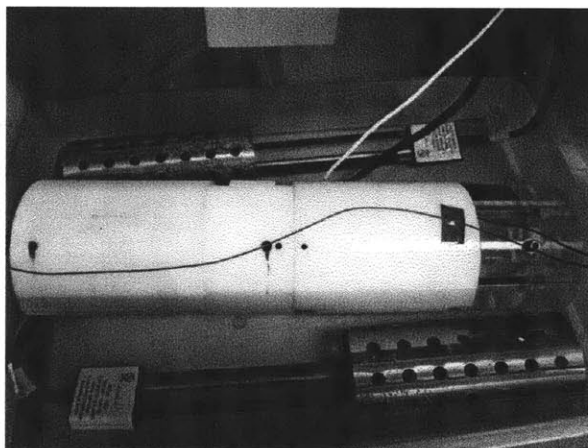
7.2 Test result

Figure 7-4: Water tank with prototype

The prototype consists of the 3X large scale polyethylene prototype with an imbedded ball valve and SMA, turbidity sensor connected to the microprocessor, and PCB energy storage/delivery board. The whole system is immersed in the constant temperature water tank. We drop water through the valve orifice to simulate the data during backflow event. After the turbidity data change is picked up by the sensor, the microprocessor starts the charging stage on the PCB board. After the initial decision, the system will keep charging until the actuation, even if the fluid flow in the orifice stops. It takes up to 200s to finish charging the capacitors and less than 0.5s to finish turning the ball valve for 90 degrees to completely shut down the production valve. The wire will cool down to ambient $60°C$ within 10s, and the SMA wire will hold the ball valve position and production valve closed. The real time ball valve angle would behave as shown in Figure 7-5. It is zero during the charging stage, goes to 90 degrees within 1s, and remains closed thereafter.
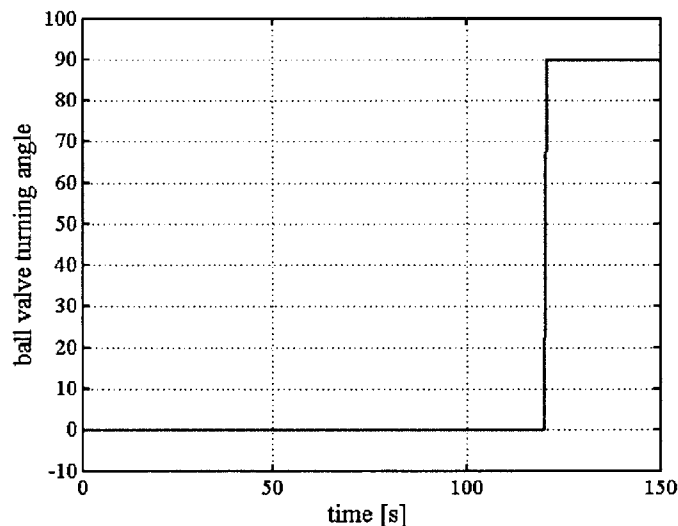
Figure 7-5: Ball valve turning angle during actuation

In the experiments, sometimes the ball valve did not successfully finish a complete turn due to the large friction at the bearing. We should pay special attention to the tolerance and corrosion protection of ball valve bearing.

This test proves that the electronically-actuated smart safety valve could function as designed in the production environment and shut down the production valve during emergency backflow.

91

Chapter 8

SMA Repeatability Test

Fatigue can be an issue for the reliability for any application dependent on the material characteristics. For our safety valve, the shape memory alloy is in low tension before actuation and contracts only once. The production valve has to be retrieved from the tubing and replaced after each malfunction event. Fatigue is not a significant issue. However, we still want to understand its behavior with multiple cycles in case we want to implement more mechanisms and keep using the valve after a backflow event. Johnson Matthey [4] performed a comprehensive study of fatigue and permanent deformation of NiTi. Permanent strain tends to occur only to a small degree in most applications where significant stress (over 138 Mpa) is involved during shape memory recovery. In general, this strain will be less than 5%, even after a million cycles, and most of it occurs within the first few hundred cycles. For specially processed materials, such as Flexinol wire from Dynalloy, the accumulated strain after a million cycles may be a little as 0.5% or less [4].

We could find no published articles on particular experiments to test fatigue performance. We designed a test to prove that our system can function after a significant number of cycles. Our system, including the safety valve prototype and the SMA wire, is stored in a large bucket with a small hole at the bottom connected to a recycle bucket(Figure 8-1). Hot water is constantly pumped into the bucket until it's full and the prototype is completely immersed. Then a slow flow of hot water keeps the water level and tank temperature constant as water drains from the bottom hole. To complete one cycle, it takes about half an hour to heat up the valve body and additional 10 minutes to heat up the memory wire inside. The cooling process is similar, with ice water pumped into the bucket. This test equipment cannot finish high frequency tests if we want to run over 100 cycles within 24 hours.

8.1 Test Facility

We built a brand new high frequency test equipment (Figure 8-1). It tests the behavior of the memory alloy alone, and is in direct contact with the heating/cooling fluid. The test piece is an SMA tube with a 0.09 inch diameter from Johnson Matthey [4]. It is mounted on a 1/8-inch

aluminum tube and clamped at the bottom on the 80/20 aluminum frame. The tube top is connected to a counter weight with a level-pulley mechanism. The weight preloads the wire with a 30 Mpa tension, below the actuation tension, 172 Mpa. We inserted a National Instrument fast response temperature thermocouple probe through the pipe and connected it to the Labview data monitor system. Two large buckets hold ice water and hot water respectively. One heat exchanger is constantly heating up the hot water. The temperatures are kept at $25°C$ and $80°C$ respectively. One temperature probe monitors the temperature in the hot bucket constantly. Two small 1GPM water pumps are controlled by the Labview system and alternate with a 30s interval to pump hot/cold water through the aluminum tube. With this frequency, the wire can finish one complete cycle, contraction and expansion, 60 times in one hour. During the contraction stage, the memory alloy tube will contract and pull the counter weight through the lever-pulley mechanism. The angle sensor mounted on the lever will record the lever angle change and convert it to the amount of tube contraction. A larger angle value indicates a large amount of contraction. An ideal SMA would have negligibly small change of contraction after thousands of cycles [4].

One major challenge is the large heat inertia of the thermocouple probe. A thermocouple consists of two dissimilar conductors in contact, which produce a voltage when heated. The size of the voltage is dependent on the difference between the temperature of the junction and other parts of the circuit. Thermocouples are a widely used type of temperature sensor for measurement and control. The thermocouple we used has a metal shield wrapping the copper and aluminum wires inside. It takes up to 1 minute to heat up the shield and reach temperature equilibrium with the ambience before the thermocouple can be heated. Also, the thermocouple was inserted directly in the water bucket. However, there is always a significant delay between the SMA wire and water temperatures. We had to leave enough time (typically over one hour) to ensure that the thermocouple data converges and settles down to the real wire temperature. In the new system, we remove the outer shield and the thermocouple metal wires are in direct contact with the inner surface of the memory alloy tube to synchronize the temperature change.
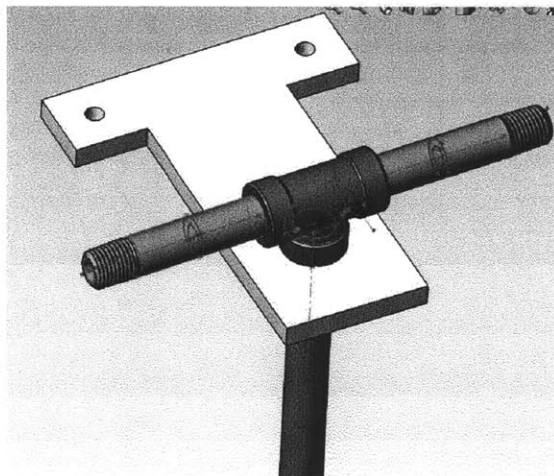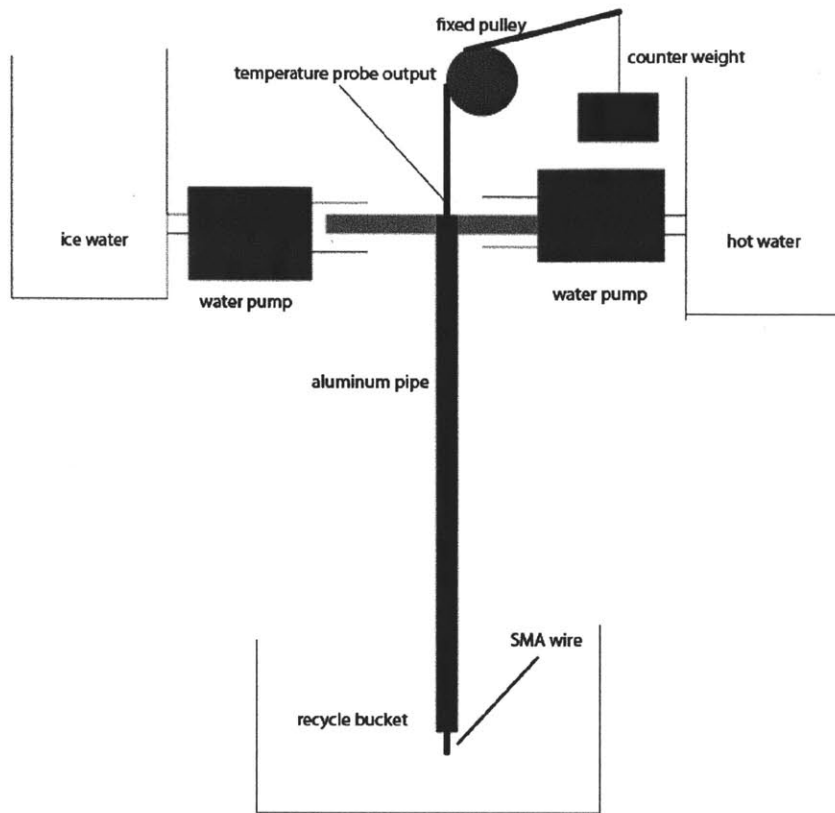
fixed pulley

counter weight

temperature probe output

ice water

hot water

water pump

water pump

aluminum pipe

SMA wire

recycle bucket

Figure 8-1: High frequency test equipment design

8.2 Test Result

Figure 8-5 shows that the total contraction amount is fairly stable through cycles. The SMA tube was clamped to the 80/20 aluminum frame at the bottom and tied with a knot at the top with a wire connected to the lever. The angle sensor data on the lever was recorded to represent the contraction amount.
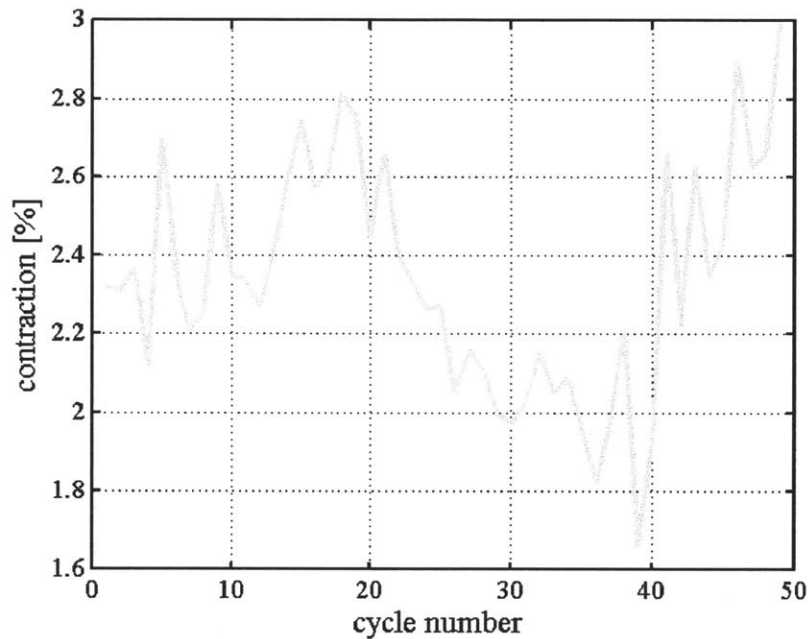
Figure 8-5: Total contraction amount for each cycle

The test results shown in Figure 8-5 show that the contraction/expansion performance varies within a tolerable range. The contraction variation is mostly due to the heating water temperature, not the mechanical fatigue or permanent strain of the material itself. We conclude that this fatigue performance is more than satisfactory for our purpose, which runs only once for the current design and probably not run more than 10 cycles for future designs.

8.3 Chapter summary

We repeated experimentally previous studies on the permanent strain due to multiple cycles. The design of a high frequency cooling and heating system for memory alloy tube and synchronized temperature data collection was detailed. We draw a conclusion that the shape memory alloy contraction through multiple cycles stays within a tolerable region.

Chapter 9

Conclusion

This thesis has reviewed the previous safety mechanisms for a gas lift valve and identified a major technical challenge of well temperature fluctuation that needs to be addressed before this technology can be brought to market. Our solution—an electronic sensing and logic system—was designed, manufactured, and tested in a controlled environment with a proof-of-concept prototype. Preliminary experiments on the system's survival ability were performed.

9.1 Summary

In Chapter 1 we first reviewed the current world oil production situation and emphasized the increasingly important status of gas lift technology in delaying the US oil production peak. Prior art in thermally-actuated safety mechanisms for gas lift valves was introduced, and we described one major design improvement needed to finalize it. We introduced the shape memory alloy technology and explained how it is applied. Temperature drift in the oil reservoir is a major design challenge and meeting this challenge was the fundamental motivation for this thesis. Some design spaces and assumptions were listed in order to simplify the design frame.

Chapter 2 described the possible solutions we explored. Their advantages and disadvantages were presented and analyzed.

Chapter 3 presented the major design solution that we worked on. The electronically-actuated sensing-logic system was described and analyzed at both the system level and component level. The quantitative requirements for each part and for the system were calculated and documented. Methods to minimize the circuit volume and to custom fashioning the system were discussed. The way to integrate the design with the current valve technology was investigated: one concept for the valve annulus chamber turned out to be a suitable way to approach the problem.

Chapter 4 modeled shape memory alloy wire in both heat transfer and structural strength. We proved that the shape memory wire system can function well in both air and water, and we obtained quantitative results of the timing and temperature range for actuation. In addition, the tuning tension proved insignificant for permanent strain.

Chapter 5 detailed the sensors chosen for implementation in the electronic system. The off-the-shelf parts were presented, and their measurement mechanisms were explained in detail.

Chapter 6 discussed survivability testing on both the component level and the system level to demonstrate that the electronic system can function and stay alive within our required time frame. Improvements to battery technologies were suggested as areas for future work, and manufacturing details were presented.

Chapter 7 documented a complete system functionality test, with the shape memory alloy actuation system, control circuit with energy storage, microprocessor, and sensors, as well as the prototype valve body in a controlled-temperature tank to simulate the downhole environment. Occasional failure and its failure mode were analyzed, and improvements were suggested.

Chapter 8 repeated experimentally previous studies on the permanent strain due to multiple cycles. The design of a high frequency cooling and heating system for memory alloy tube and synchronized temperature data collection was detailed.

9.2   Future work

Gas lift technology is being applied to increasingly deeper wells. Currently, production pressure can go up to 15000 psi. In addition, instead of pumping gas into tubing with multiple valves, drilling technology has evolved to implement a single injection method to save both drilling and maintenance costs. More research needs to be done on improving safety valve performance and reliability under high pressure.

With our design, the valve has to be tuned to fit each particular well before installation since the production mean temperature varies significantly between different wells. Sometimes, onshore estimation and simulation may yield results with a large degree of error, and on-site data collection can be expensive. The next step is to design a universal safety valve that could fit all wells. It could be a variation based on the current shape memory alloy scheme or it could replace the actuation mechanism with a completely different technology.

Battery technology is still the bottleneck for any electronic downhole device. The lithium battery is prone to fire and explosion. Future improvements could focus on searching for a high energy density, low self-discharge rate battery that can survive under high pressure and temperature. Another improvement may entail wrapping the lithium battery to make it more robust

in the harsh downhole environment. Deep sea battery cell technology is quite mature with multiple companies in the market, but they rarely manufacture heavy duty batteries with our size and voltage. Further cooperation may be established if this design concept could be accepted by the market. One other path to pursue is the application of primary cell, which has electrodes and electrolytic solution unmixed before activation and only provide voltage and current after the individual parts are mechanically connected.

Another trend in gas lift industry is decreasing size and versatility of gas lift valves. The safety valve has to shrink in size accordingly. We have built a functional prototype with off-the-shelf parts from general distributors. We should further investigate the potential of custom making the circuit with smaller parts. Most of the parts we used are for general use with multiple other features that are not necessary for gas lift valves. By eliminating the extra feature and simplifying the system design, the total electronics volume could decrease to a lower order of magnitude.

Our design concepts including the thermally actuated version and the electronically controlled version have to go through a comprehensive integration and test with real gas lift valve and production wells. The industrial experiment could be carried out in three phases: first phase to assemble and test in lab facility with downhole environment and oil immersion, second phase to test the functionality at on-shore wells, and last phase to install one prototype at off-shore wells and run for up to two years. The electronic characteristics should be recorded both before and after the test for future comparison. Cooperation with oil service companies and equipment OEM's, such as Schlumberger, Weatherford and Chevron would be beneficial.